Effective Two-Body Force Inferred from the (p, n) Reaction on ^{17}O, ^{18}O, ^{27}Al, and Other Light Nuclei*

J. D. ANDERSON, S. D. BLOOM, AND CALVIN WONG
Lawrence Radiation Laboratory, University of California, Livermore, California 94550
AND
W. F. HORNYAK
University of Maryland, College Park, Maryland
AND
V. A. MADSEN
Oregon State University, Corvallis, Oregon

(Received 8 August 1968)

Using the Livermore variable-energy cyclotron time-of-flight facility, the angular distribution of the neutrons from the (p, n) reaction on ^{17}O, ^{18}O, and ^{27}Al has been measured in 15° steps from 0° to 135° for 13 proton energies between 7 and 13.5 MeV. The persistence of a rather large $^{18}O(p, n)^{18}F$ ground-state reaction ($\Delta T=1$, $\Delta J=1$) over the entire energy region studied clearly indicates the operation of a spin-flip mechanism in the effective two-body force. The ^{18}O and $^{17}O(p, n)$ isobaric cross sections ($\Delta T=0$, $\Delta J=0$) are experimentally observed to be roughly equal, while optical-model calculations (including the isospin potential) predict ^{18}O cross sections to be twice as large as those for ^{17}O. This disagreement can be qualitatively explained by the presence of a large spin-flip term in the effective two-body force. The $^{17}O(p, n_1)^{17}F^*$ ($J_i=\frac{5}{2}^+$, $J_f=\frac{1}{2}^+$) and the $^{18}O(p, n)^{18}F^*$ ($\Delta T=0$, $J_i=0^+$, $J_f=2^+$) cross sections indicate a sizeable value for the quadrupole term in the multipole expansion of the effective two-body force. These data and other light-nucleus data are analyzed using the distorted-wave Born approximation to yield an estimate of the effective central two-body interaction. For an assumed Yukawa force with a range of 1.4 fm, this analysis yields $V_\tau \simeq 9$ MeV and $V_{\sigma\tau} \simeq 6$ MeV. A comparison is made between these force constants and those obtained from other sources.

I. INTRODUCTION

THE possibility of obtaining information about the effective residual two-body force in nuclear matter from studying nuclear reactions is well known.[1–3] The (p, n) reaction is a sensitive probe of the part of the two-body force involving the charge-exchange operator P_τ.[4,5] Recently, we reported some preliminary results on the direct (p, n) reaction in the cases of ^{17}O and ^{18}O. These results show that the charge-exchange part of the effective two-body interaction consisted of roughly equal parts (1:2) of spin-dependent and spin-independent amplitudes.[6] Although one can qualitatively draw conclusions from an inspection of cross-section measurements alone,[6] quantitative analysis of the data requires the use of a model. In the present analysis, use is made of the distorted-wave Born approximation (DWBA) with a finite-range, central, two-body force neglecting space exchange.[7] These DWBA calculations are applicable to both analog and other transitions.

The target nucleus ^{17}O was selected to complement previous (p, n) measurements on ^{15}N. This choice provides nuclei which could be described as a core+nucleon (or hole), but with different nucleon configurations so as to determine the sensitivity of the results to the shell-model configuration of the target. As will be shown, the shape of the angular distribution for the low-energy direct (p, n) reaction (<25 MeV) is relatively insensitive to target structure except for size effects. However, the total cross section can be expressed as the incoherent sum of two parts, one due to pure charge exchange and the other due to simultaneous charge and spin exchange. In analog transitions between states of nonzero spin, the spin-independent part is insensitive to details of the wave function, whereas the spin-dependent part is sensitive to the j value of the single-particle orbit.[8] The ^{18}O study was not only required for background measurements (since ^{18}O is a contaminant in the ^{17}O measurements), but also provides direct evidence, from the J^π $0^+ \rightarrow 1^+$ transitions, for the existence of the spin-flip reaction.

An assumption which is implicit in the present analysis is that the (p, n) reaction is indeed proceeding via a direct-reaction mechanism. To establish the reaction mechanism, angular distributions were measured for proton bombarding energies of 7–14 MeV. Having investigated the energy dependence of the cross sections, we found that only the highest-energy data were suf-

* Work performed under the auspices of the U.S. Atomic Energy Commission.

[1] For an excellent review of this approach, see G. R. Satchler, Nucl. Phys. **A95**, 1 (1967).

[2] S. D. Bloom, N. K. Glendenning, and S. A. Moszkowski, Phys. Rev. Letters **3**, 98 (1959).

[3] C. Wong, J. D. Anderson, S. D. Bloom, J. W. McClure, and B. D. Walker, Phys. Rev. **123**, 598 (1961).

[4] G. R. Satchler, R. M. Drisko, and R. H. Bassel, Phys. Rev. **136**, B637 (1964).

[5] J. B. French and M. H. Macfarlane, Phys. Letters **2**, 255 (1962).

[6] S. D. Bloom, J. D. Anderson, W. F. Hornyak, and C. Wong, Phys. Rev. Letters **15**, 264 (1965).

[7] W. R. Gibbs, V. A. Madsen, J. A. Miller, W. Tobocman, E. C. Cox, and L. Mowry, NASA Technical Report No. TN D-2170, 1964 (unpublished).

[8] This is analogous to the wave-function dependence of Fermi and Gamow-Teller matrix elements in β decay.

ficiently free of fluctuations to justify the use of the direct-reaction model.

We assume that the charge-exchange part of the effective two-body force is represented by

$$V_{0i}=\tau_0\cdot\tau_i[V_{\sigma\tau}(\sigma_0\cdot\sigma_i)+V_\tau]f(r_{0i}), \quad (1)$$

where $f(r_{0i})$ is the Yukawa form factor with a range of 1.4 fm and the subscripts 0 and i refer to the incident and struck nucleons, respectively. The selected data are then analyzed to yield absolute values for $V_{\sigma\tau}$ and V_τ. By using the formal connection between β decay and our microscopic description of the (p, n) reaction,[9] it follows that our ^{18}O results are essentially predictable from the β-decay probability of ^{18}F.

The relative importance of the multipole moments corresponding to the angular-momentum transfer is discussed and, in particular, the existence of enhanced quadrupole transitions ($\Delta L=2$) is pointed out. Since a considerable amount of work has been done on the (p, n) isobaric reaction using the macroscopic approach originally suggested by Lane,[10] a comparison is made between the predictions of the macroscopic and microscopic theories (with each other and with experimental data) and the similarities and differences in these approaches are noted.

The experimental methods and results are discussed in Secs. II and III. Section IV reviews the microscopic direct-reaction theory for charge exchange. Section V gives a qualitative description of some results of the theory and its application to several important features of the data. Section VI contains the detailed application of the theory in the analysis of data, including a tabulation of relevant parameters. In Sec. VII we discuss the results of the analysis and compare the force constants with information on the effective two-body force obtained from other sources.

II. EXPERIMENTAL METHOD

A. Geometry and Electronics

The basic electronic system and experimental geometry have been described in detail elsewhere[11] and are only briefly summarized here. For angular-distribution measurements, the Livermore time-of-flight facility has available 10-m flight paths from 0° (3°) to 135° in 15° steps. The 10-m flight paths are collimated so that the detectors directly view only a few inches around the target area, thus reducing the background from the "beam-catcher" and sweeping slits. Because of the multiple Coulomb scattering from the entrance and exit foils of the gas targets, an additional section of lead-lined beam catcher was extended into the target chamber to ensure accurate charge collection.

B. Targets

The oxygen targets were ≃150 keV thick to 10-MeV protons (10-cm length at a pressure of 380 mm Hg). The gas was contained in a low-mass cell with a 0.00025-in. tantalum entrance-and-exit window. The mass analyses for the oxygen gas targets are as follows: ^{17}O target—50.1% ^{17}O, 40.3% ^{16}O, and 9.6% ^{18}O; ^{18}O target—53.3% ^{18}O, 45.3% ^{16}O, and 1.4% ^{17}O. The aluminum target was 100 keV thick to 10-MeV protons (3 mg/cm^2) and was obtained commercially as a foil.

III. EXPERIMENTAL RESULTS

The 15° time-of-flight spectrum resulting from 8.4-MeV proton bombardment of ^{18}O is shown in Fig. 1. The neutron groups marked with asterisks in that figure correspond to unresolved levels in ^{18}F. The excitation energies[12,13] for the various neutron groups are also shown. The angular-distribution data—3°, 15°, 30°, 45°, 60°, 75°, 90°, 105°, 120°, and 135°—were obtained simultaneously in 100-channel subgroups of an 800-channel pulse-height analyzer and 128-channel subgroups of a parallel 256-channel analyzer. Typical dead-time corrections were 10%. The neutron-attenuation correction for the gas-target cells was 10%. An additional 20% absorption correction was necessary on all 15° data because of the beam-catcher insert.

The correction to the ^{17}O(p, n_0)^{17}F cross section due to the ^{18}O impurity in the ^{17}O target varied as a function of bombarding energy from 5 to 15%. Because of the difficulty in obtaining an unambiguous mass analysis (mass 34 can be obtained from both $^{17}O_2$ and ^{16}O ^{18}O molecules), a direct measurement of the ^{18}O content in the ^{17}O target was made using the ^{18}O(p, n_0)^{18}F reaction. For 7–8-MeV protons, where the ground-state cross section was sufficiently large to obtain an accurate comparison, the results confirmed the mass spectrographic analysis.

A. ^{17}O(p, n)^{17}F

The ^{17}O(p, n)^{17}F angular distributions, corrected for absorption and transformed to the c.m. system, are shown in Fig. 2. Above 12.5-MeV proton energy, the neutron group (n_1) corresponding to the first excited state ($E_{ex}=0.5$ MeV) could not be resolved from the ground-state neutrons (n_0). The inclusion of some of these neutrons in the ground-state group does not seriously alter the n_0 results, since the intensity of the n_1 group is only 20% of n_0.

The ground-state neutron angular distributions show considerable fluctuation in shape. A strong forward peaking is observed for proton energies of 9–10 and

[9] C. Wong, J. D. Anderson, J. W. McClure, B. Pohl, V. A. Madsen, and F. Schmittroth, Phys. Rev. **160**, 769 (1967).
[10] A. M. Lane, Phys. Rev. Letters **8**, 171 (1962); Nucl. Phys. **35**, 676 (1962).
[11] B. D. Walker, J. D. Anderson, J. W. McClure, and C. Wong, Nucl. Instr. Methods **29**, 333 (1964).
[12] J. W. Olness and E. K. Warburton, Phys. Rev. **151**, 792 (1966).
[13] A. R. Poletti, Phys. Rev. **153**, 1108 (1966).

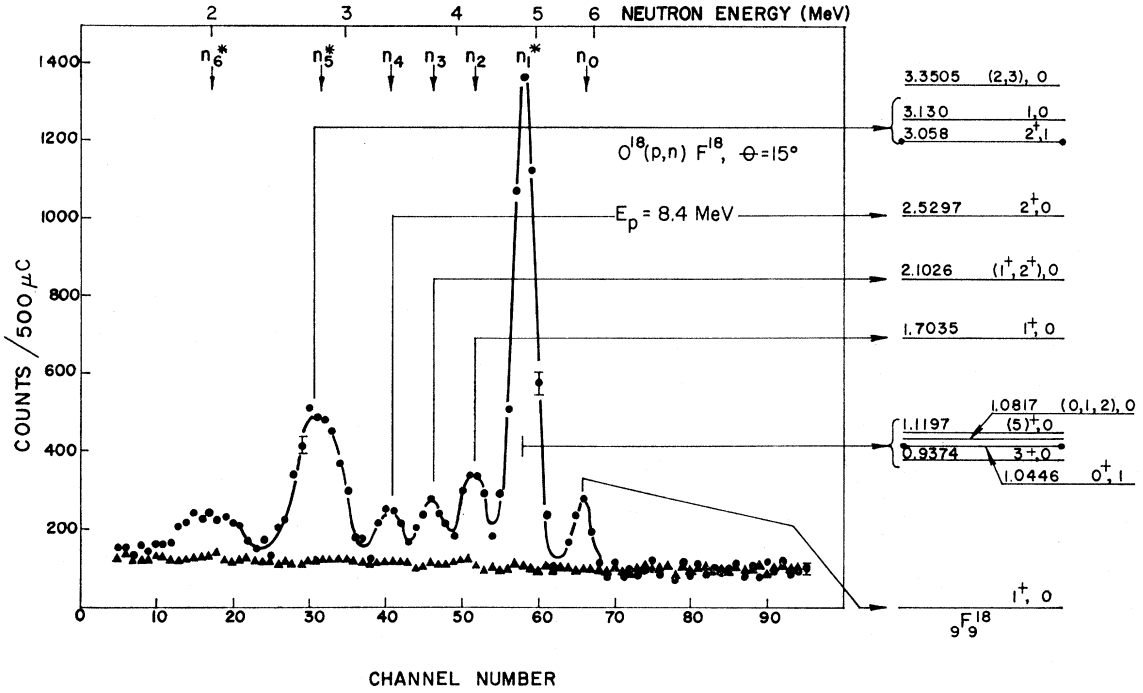

FIG. 1. 15° time-of-flight spectrum of neutrons resulting from bombardment of ^{18}O with 8.4-MeV protons. The neutron groups corresponding to final states in ^{18}F are indicated by the arrows at top right-hand side of the figure.

above 12 MeV, while the 0° cross section is generally a minimum for proton energies of 7–9 and 10.5–12 MeV. The $^{17}O(p, n_1)^{17}F^*$ angular distribution has a relatively constant shape over the energy region measured with a maximum in the cross section at about 50° and a minimum at 0°.

In Fig. 3 the integrated cross sections are shown as a function of proton bombarding energy. The energy dependence of the n_0 and n_1 cross sections are quite similar and the ratio of n_0 to n_1 is approximately 5, independent of bombarding energy. For the ground-state cross section (n_0), there is a correlation between the inverted shape of the angular distributions (minima at 0°) and the maxima in the energy dependence of the integrated cross section. This is most evident at 10.8-MeV bombarding energy.

B. $^{18}O(p, n)^{18}F$

In the following discussion we shall refer to the neutron group n_1 as corresponding to the isobaric state ($T=1$), although it contains contributions from other close-lying levels (see Fig. 1). Similarly, we shall refer to n_5 as corresponding to the $J=2^+$, $T=1$ state in ^{18}F at 3.06-MeV excitation energy. The contribution of the unresolved levels to these cross sections will be discussed elsewhere. Above 10-MeV bombarding energy, neutron groups n_2, n_3, and n_4 are not individually resolved. Above 12 MeV there may be some small additional uncertainty in the n_1 group due to the contribution of n_2.

The $^{18}O(p, n)^{18}F$ ground-state (n_0) and isobaric-state (n_1) angular distributions are shown in Fig. 4. Over most of the energy region studied the n_0 and n_1 angular distributions are quite similar, the notable exceptions being between 7- and 9-MeV bombarding energies. The integrated cross sections are shown as a function of bombarding energy in Fig. 5. The ratio of n_1 to n_0 is strongly energy-dependent, varying from 3 at 7 MeV to 8 at 12 MeV.

In Fig. 6, angular distributions are shown for neutron groups n_2, n_3, n_4, and n_5. The angular distributions for n_2, n_3, and n_4 are somewhat similar but bear little resemblance to the ground-state group n_0. The angular distribution for n_5, particularly at higher energies, shows a minimum cross section at 0° and a maximum around 50°, which is quite similar to the $^{17}O(p, n_1)^{17}F^*$ angular distribution.

The integrated cross section for neutron group n_5 (see Fig. 5) is about half the isobaric cross section n_1 independent of bombarding energy. Groups n_2, n_3, and n_4 have cross sections roughly comparable to the ground-state cross section n_0 and have the same energy dependence over the rather limited range of the measurements. From the integrated cross sections one notes that the isobaric ($\Delta T=0$) cross section (n_1) and the isobaric 2^+ cross section (n_5) have the same energy dependence. The isospin-flip ($\Delta T=1$) cross sections (n_0, n_2, n_3, and n_4) have roughly the same energy dependence among themselves but are different than those for $\Delta T=0$.

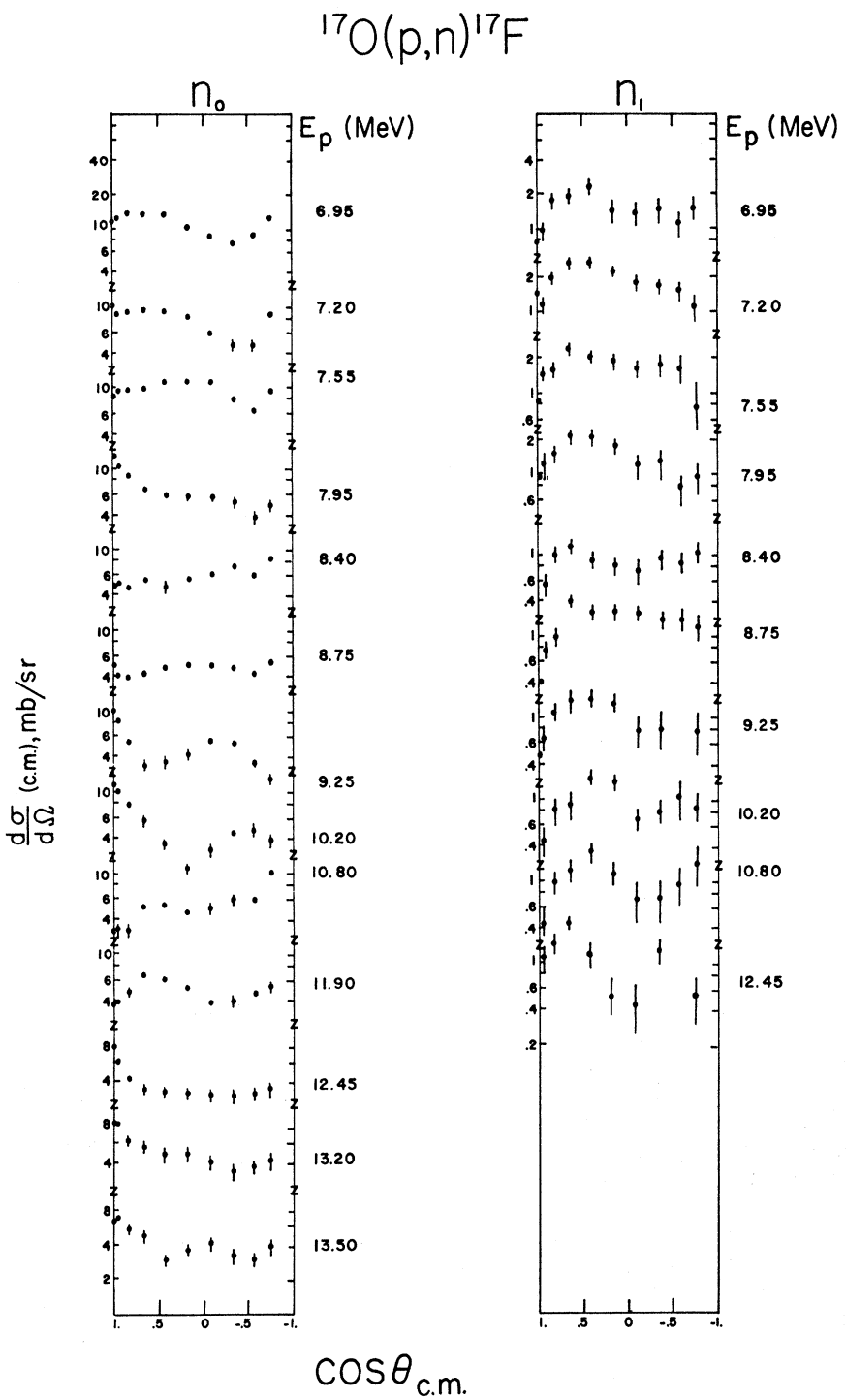

FIG. 2. Angular distributions for $^{17}O(p, n)^{17}F$ for ground-state (n_0) and first-excited-state (n_1) neutron groups. E_p is the laboratory energy.

C. $^{27}Al(p, n)^{27}Si$

The $^{27}Al(p, n)^{27}Si$ angular distributions are shown in Fig. 7. Whenever the detector efficiency (due to the neutron energy change as a function of angle) was large enough to cause appreciable uncertainties in the angular-distribution data (>20%), the data were omitted—thus the smaller angular range of data for the lowest proton bombarding energies. For the ground-state reaction (n_0), the angular distribution below 9-MeV bombarding energy is rather isotropic; around 9 MeV, the 0° cross section is a minimum, with the

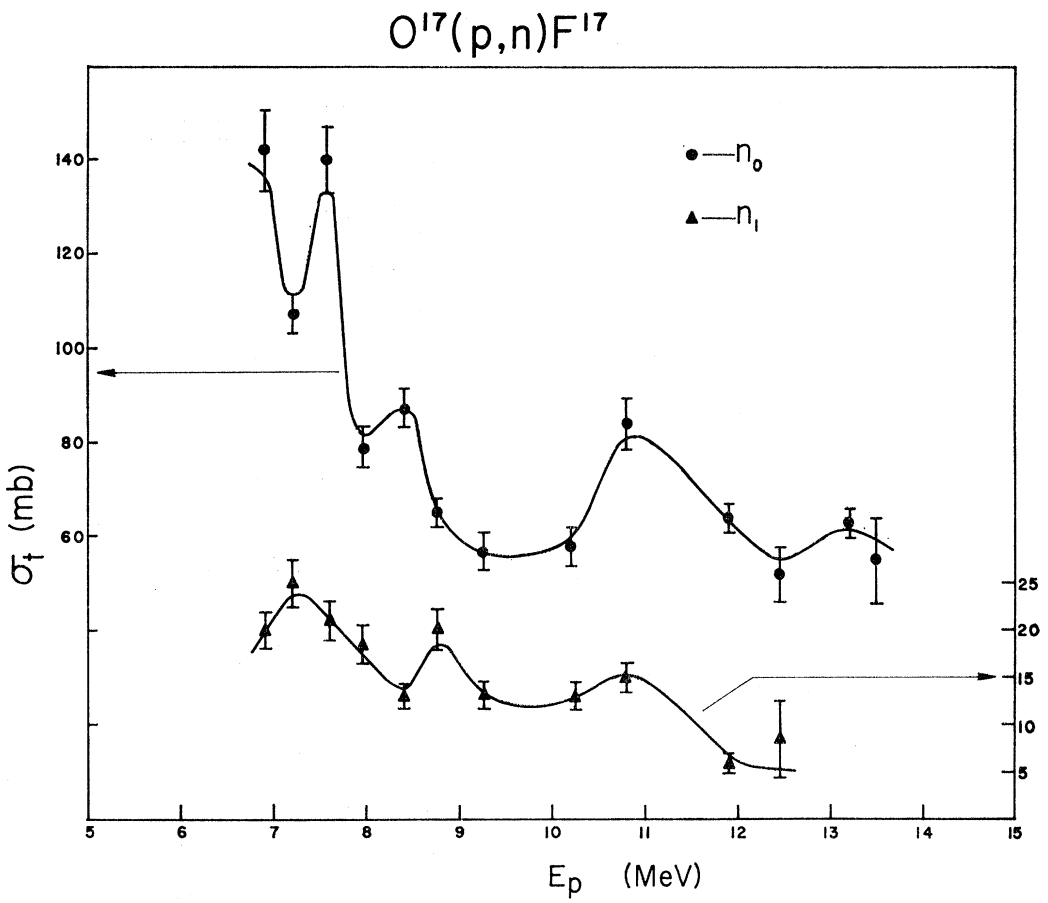

FIG. 3. Integrated cross sections for $^{17}O(p, n)^{17}F$ for ground-state (n_0) and first-excited-state (n_1) neutron groups. (Solid lines are for guidance only; note different scales on ordinates.)

maximum cross section at 60°; and above 10 MeV, the angular distribution is forward-peaked.

Although neutron group n_1 is resolved from n_2 at only a few energies, the n_1 angular distribution is similar to the $^{17}O(p, n_1)^{17}F$ cross section, having a minimum at 0° and a maximum at about 60°. The angular distributions for the sum of groups n_1 and n_2 fluctuate in shape but are generally forward-peaked.

The integrated cross sections are shown in Fig. 8. The n_0 data below 7 MeV were taken by Hansen *et al.*[14] with a "long counter." Over the energy region where the neutron groups n_1 and n_2 are resolved, the neutron group n_2 is roughly twice as large as n_1. The ratio of n_0 to n_1 is approximately 4.

IV. THEORY

Recently, several treatments of direct inelastic scattering have appeared.[15–17] Here, we summarize the main results of Ref. 15 applied to the (p, n) reaction. The differential cross section is given by

$$d\sigma/d\Omega = (2m/4\pi\hbar^2)^2(k_f/k_i)[2(2J_i+1)]^{-1} \times \sum_{II'LM}(2I+1)(2I'+1) \times \Big|\sum_{j_1j_2} D_{j_1j_2}(II'L)F_{LM}^{j_1j_2}(\theta)(2L+1)^{-1/2}\Big|^2, \quad (2)$$

where

$$D_{j_1j_2}(II'L) = 4(2j_1+1)^{1/2}\langle l_2 \| Y_L \| l_1\rangle \times \begin{pmatrix} j_1 & \frac{1}{2} & l_1 \\ j_2 & \frac{1}{2} & l_2 \\ I & I' & L \end{pmatrix} S(J_iJ_fI; T_iT_f1; j_1j_2) \times C(T_iT_f1; P_i-P_f1)(\delta_{I'1}V_{\sigma\tau}+\delta_{I'0}V_\tau). \quad (3)$$

In Eq. (2), $F_{LM}^{j_1j_2}$ is the distorted-wave matrix element[18] for single-particle transition $j_1 \to j_2$, given by

$$F_{LM}^{j_1j_2}(\theta) = \langle \chi_f^{(-)} \mid g_L^{j_1j_2}Y_L^M \mid \chi_i^{(+)}\rangle, \quad (4)$$

[14] L. F. Hansen, M. L. Stelts, and J. J. Wesolowski, Phys. Rev. **143**, 800 (1966).
[15] V. A. Madsen, Nucl. Phys. **80**, 177 (1966).
[16] G. R. Satchler, Nucl. Phys. **77**, 481 (1966).
[17] N. K. Glendenning and M. Véneroni, Phys. Letters **14**, 228 (1965); N. K. Glendenning, Phys. Rev. **144**, 829 (1966).
[18] W. Tobocman, *Theory of Direct Nuclear Reactions* (Oxford University Press, New York, 1961).

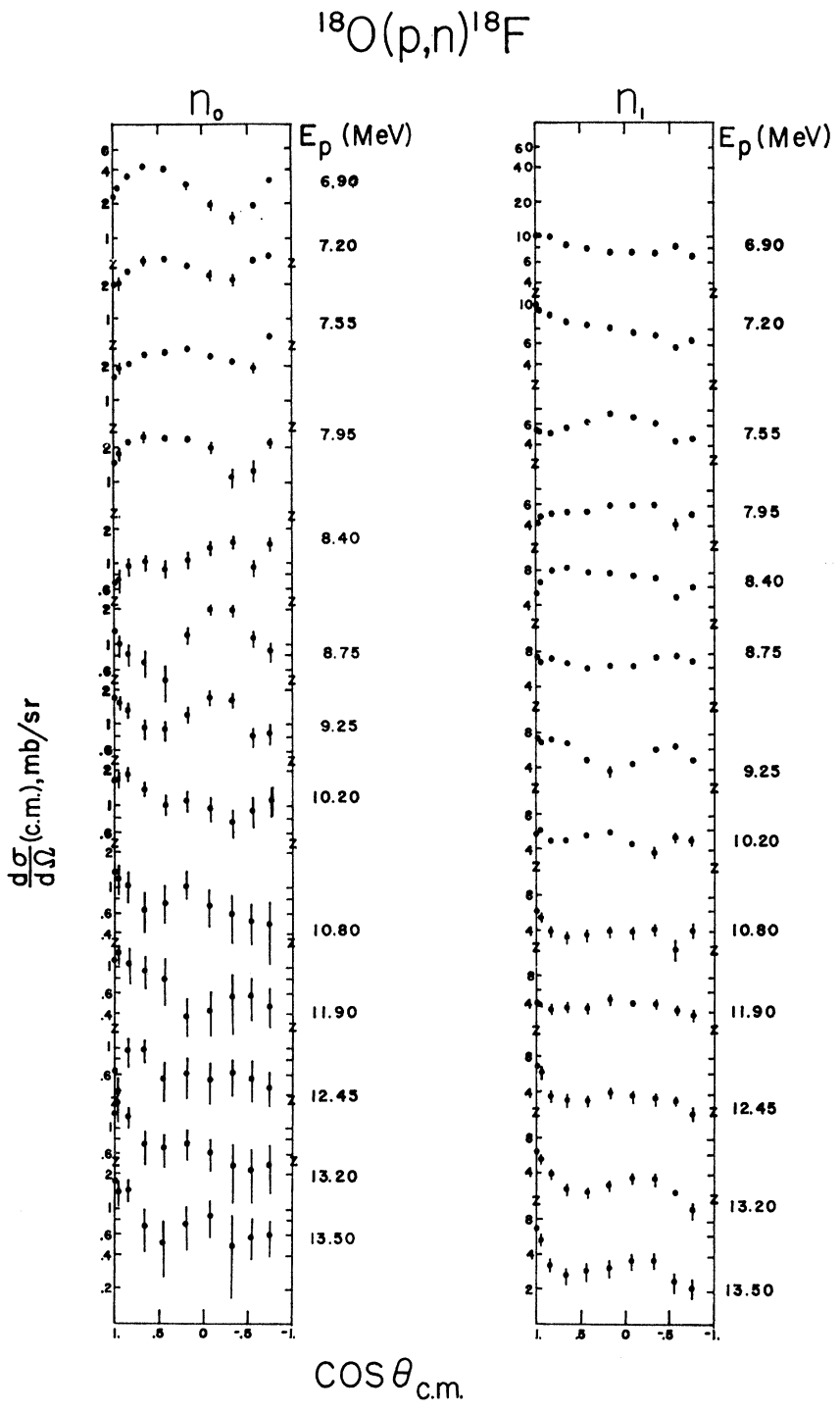

FIG. 4. Angular distributions for $^{18}O(p, n)^{18}F$ for ground-state (n_0) and analog-state (n_1) neutron groups (see Fig. 1).

with the form factor

$$g_L^{j_1 j_2} = \int R_{j_2}(r') \nu_L(r, r') R_{j_1}(r) d^3r, \qquad (5)$$

where ν_L is the radial harmonic of the interaction-potential form factor $f(r_{0i})$, V_τ and $V_{\sigma\tau}$ are strength parameters in the interaction

$$V(0, i) = \tau_0 \cdot \tau_i [V_\tau + V_{\sigma\tau} \sigma_0 \cdot \sigma_i] f(r_{0i}),$$

and $S(J_i J_f I: T_i T_f 1: j_1 j_2)$ is the spectroscopic amplitude.[15] The spin-dependent part of the interaction, Eq. (1), contributes only to those terms in Eq. (2) for which the spin transfer $I' = 1$, while the spin-in-

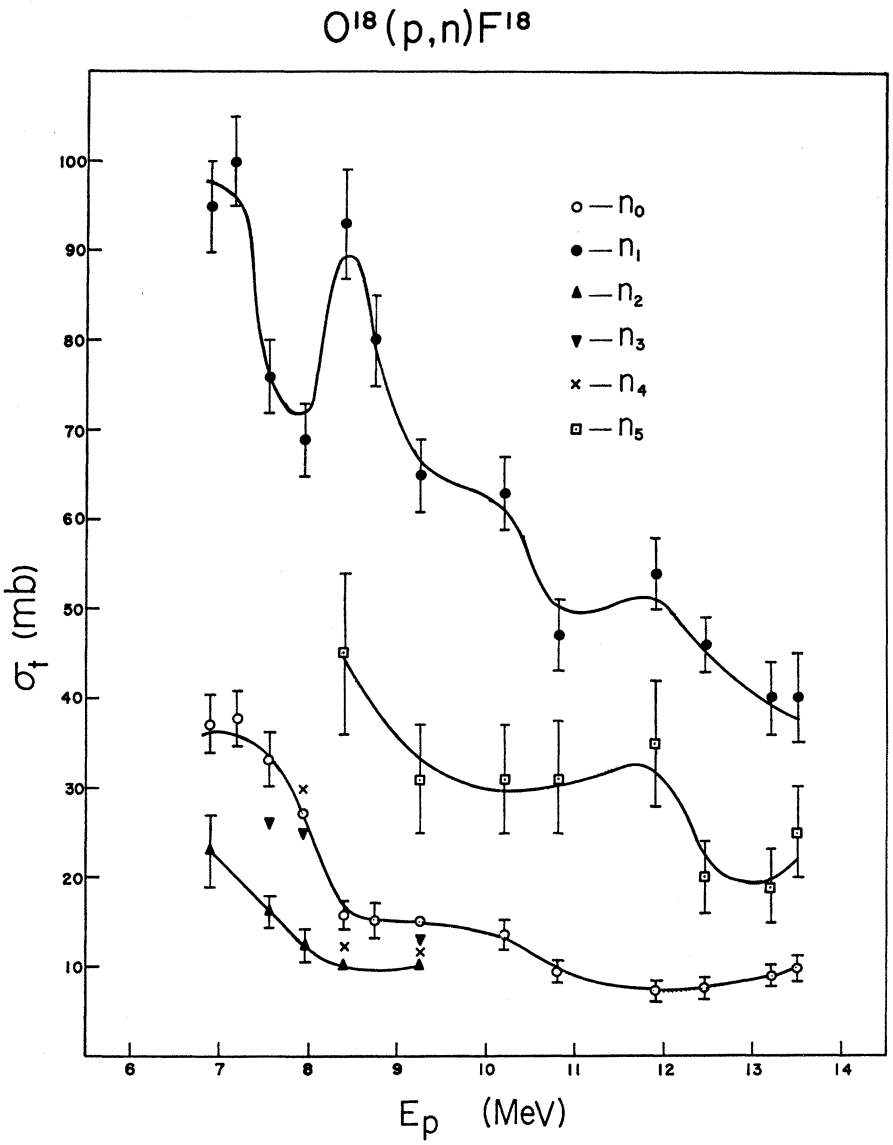

FIG. 5. Integrated cross sections for $^{18}O(p, n)^{18}F$ for various final states (see Fig. 1).

dependent term contributes terms for which $I'=0$. The $9-j$ coefficient and the spectroscopic amplitude in Eq. (3) give the following restrictions on the various quantum numbers:

$$|J_f-J_i|\leq I\leq J_i+J_f, \tag{6}$$

$$|j_2-j_1|\leq I\leq j_1+j_2, \tag{7}$$

$$0\leq I'\leq 1, \tag{8}$$

$$|l_2-l_1|\leq L\leq l_1+l_2, \tag{9}$$

$$|L-I'|\leq I\leq L+I', \tag{10}$$

and

$$|T_f-T_i|\leq \tau\leq T_i+T_f, \tag{11}$$

while the reduced matrix elements in Eq. (3) and conservation of parity in the nuclear states give the parity restriction

$$\pi_f\pi_i=(-1)^{l_1+l_2}=(-1)^L. \tag{12}$$

The cross section, Eq. (2), consists of an incoherent sum of contributions from the angular-momentum transfers I', L, and I—each of which consists of a coherent sum of angle-dependent single-particle amplitudes weighted with the coefficients $D_{j_1j_2}$. These coefficients contain the information about single-particle couplings and about the details of the nuclear wave function in the spectroscopic amplitude factor.

V. QUALITATIVE DISCUSSION

In this section we present some special cases of the theory, in order to make qualitative statements about the implications of the experimental results.

If we apply Eq. (2) to analog transitions in even nuclei, the vector inequalities (6), (10), and (12) re-

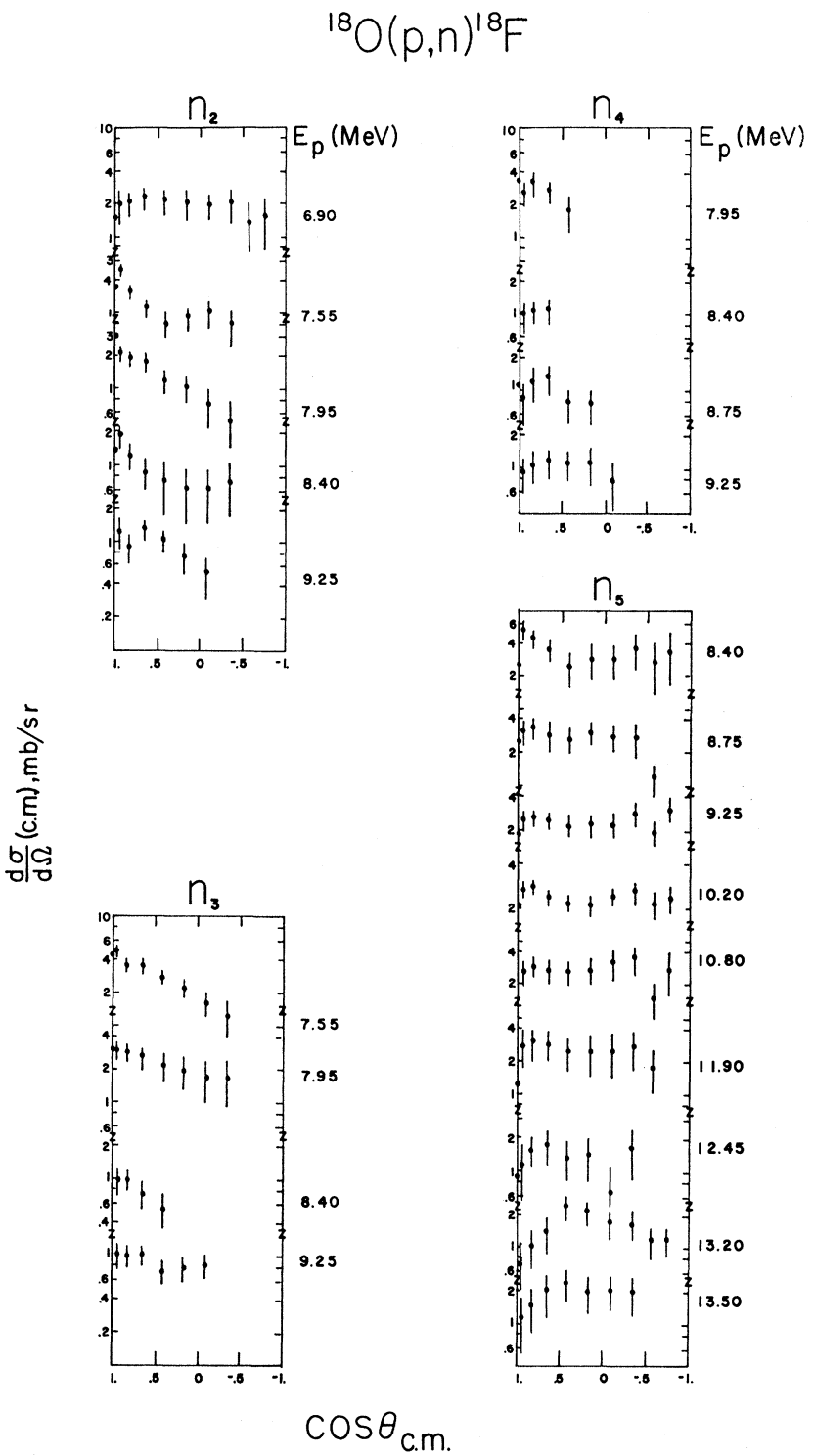

FIG. 6. Angular distributions for $^{18}O(p, n)^{18}F$ for neutron groups n_2, n_3, n_4, and n_5 (see Fig. 1).

strict the transfer quantum numbers to $I=0$, $L=0$, and $I'=0$, respectively. In this case, Eq. (2) reduces to

$$(d\sigma/d\Omega) = (2m/4\pi\hbar^2)^2(k_f/k_i)\,(V_\tau^2/\pi)\,(N-Z)^{-1} \times \left|\sum_j \langle N_i - Z_j\rangle F_{00}{}^{jj}\right|^2. \quad (13)$$

This expression also applies to odd nuclei for the $I=0$ part of the cross section, which would be dominant if the spin-flip strength $V_{\sigma\tau}$ were small. It is usually true that, for the important j subshells within a major shell, the single-particle amplitude is roughly independent of j. Let us then take $F_{00}{}^{jj} \approx F_{00}$, where F_{00} is an average

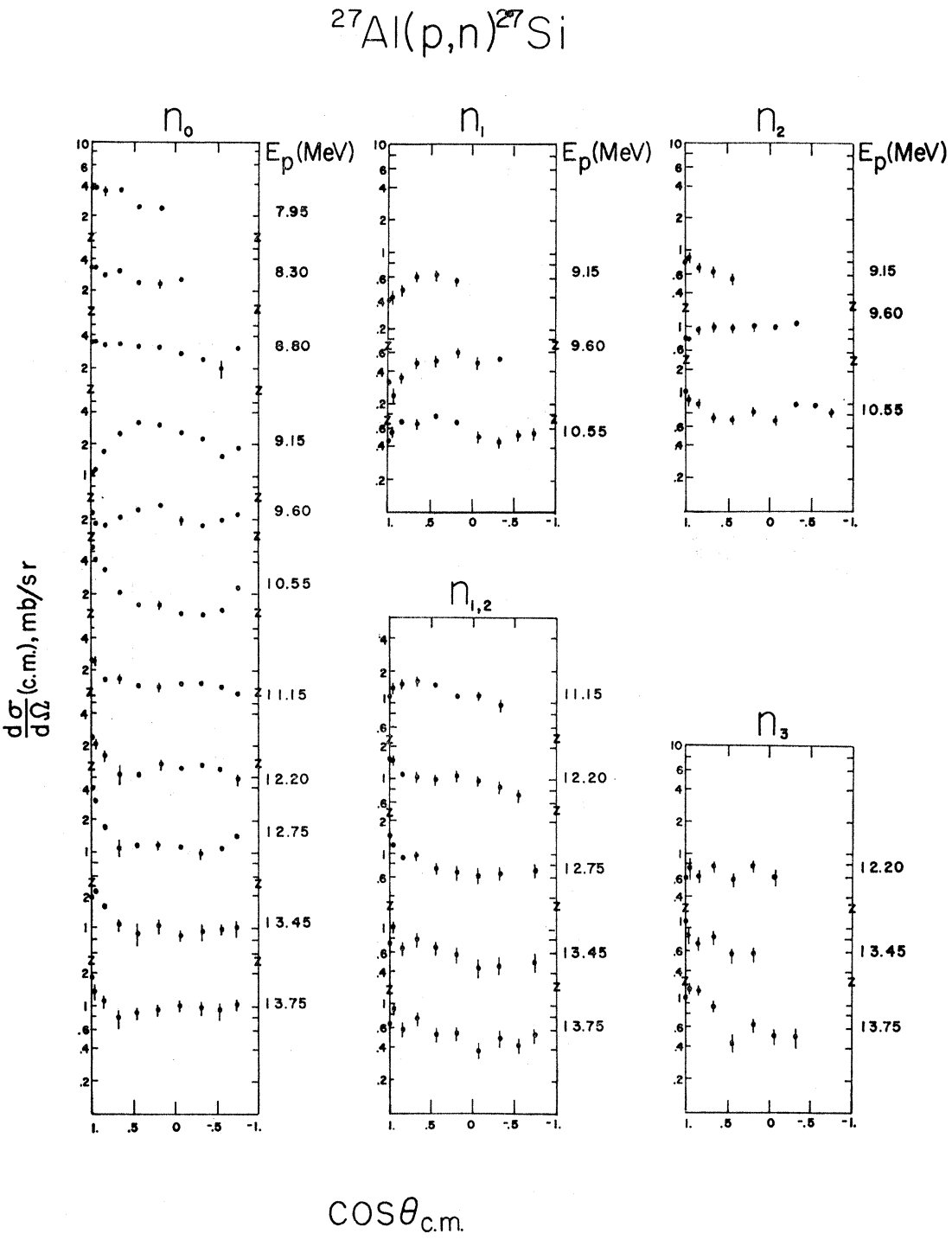

FIG. 7. Angular distributions for ^{27}Al(p, n) ^{27}Si for the following neutron groups: (a) n_0, ground state ($\frac{5}{2}^+$); (b) n_1, first excited state ($\frac{1}{2}^+$, 0.782 MeV); (c) $n_{1,2}$, first and second excited states unresolved (2nd=$\frac{3}{2}^+$, 0.958 MeV); (d) n_2, second excited state; and (e) n_3, third excited state ($\frac{7}{2}^+$, 2.165 MeV). Assignments are taken from M. B. Lewis, N. R. Roberson, and D. R. Tilley, Phys. Rev. **163**, 1238 (1967); B. H. Wildenthal and E. Newman, *ibid.* **167**, 1027 (1968).

amplitude. The j sum in Eq. (13) can be evaluated to give

$$d\sigma/d\Omega = (2m/4\pi\hbar^2)^2(k_f/k_i)(V_\tau^2/\pi)(N-Z)\,|\,F_{00}\,|^2. \quad (14)$$

The approximation made in obtaining Eq. (14) is particularly good for the $1p_{3/2}$ and $1p_{1/2}$ shells. In this approximation, the $(N-Z)$ dependence of the Lane model[10] is exhibited explicitly.

Let us next consider the relationship of this result to the Lane[10] macroscopic model. The solution of the

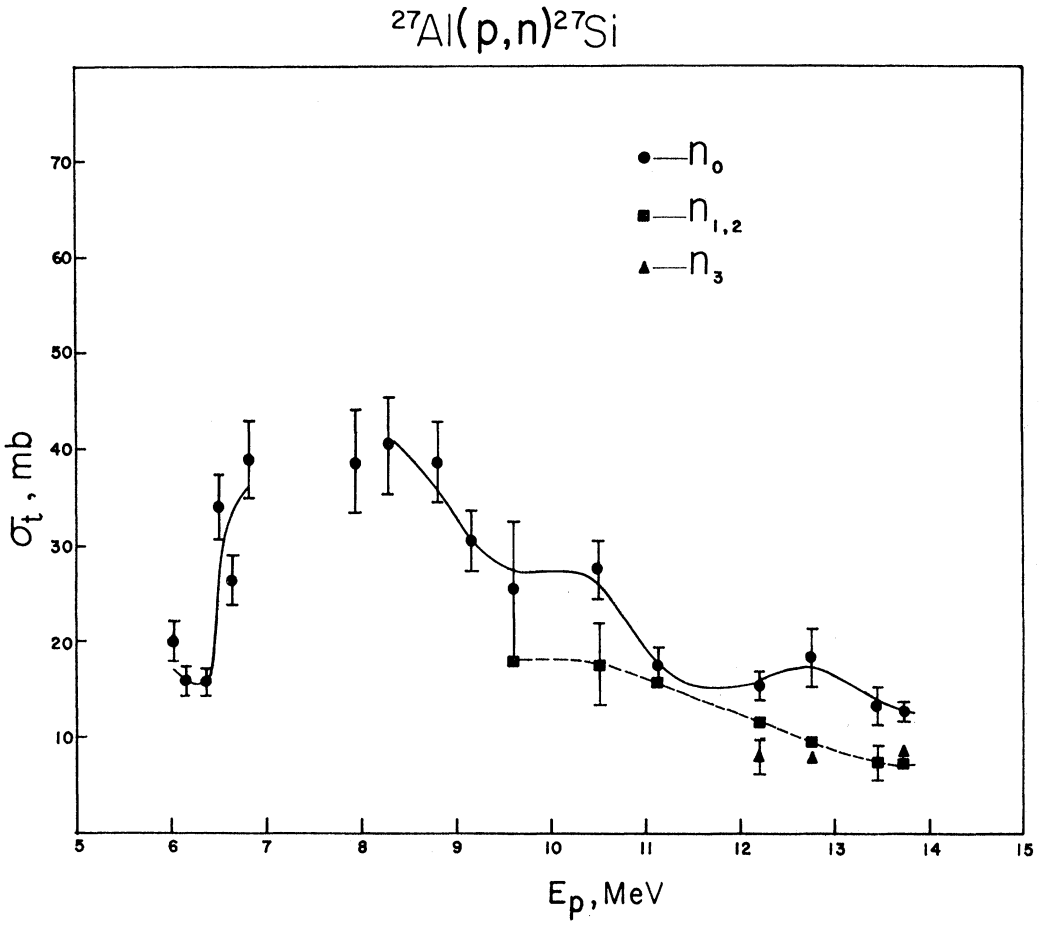

FIG. 8. Integrated cross sections for $^{27}Al(p, n)^{27}Si$ for various neutron groups.

Lane coupled equations reduces in the weak-coupling limit to the DWBA. The cross section is given by

$$d\sigma/d\Omega = (2m/4\pi\hbar^2)^2(k_f/k_i)[(N-Z)/4A^2]\,|\,F\,|^2, \quad (15)$$

where

$$F = \langle \chi_f^{(-)} \,|\, V_1(r) \,|\, \chi_i^{(+)} \rangle \quad (16)$$

is the distorted-wave matrix element of the space part of the optical-model isospin potential $V_1(r)\mathbf{T}\cdot\mathbf{t}/A$. Comparison of this result with the particle-model cross section, Eq. (14), shows that the microscopic and macroscopic pictures are equivalent in the j-independent-amplitude approximation if the macroscopic form factor $V_1(r)$ is replaced with $(A/\pi)V_\tau g_0(r)$. The mass-number dependence of Eq. (15) is contained implicitly in $g_{00}{}^{jj}$ in the normalization of the bound-state wave functions in Eq. (5); that is, $R_j(r)$ is roughly proportional to $(r_0A^{1/3})^{-3/2} = r_0{}^{-3/2}A^{-1/2}$. Thus $(A/\pi)V_\tau g_0(r)$ is roughly independent of nuclear size.

As has been shown previously in the comparison of DWBA results with the solution of the Lane equations, the charge-exchange interaction strength is sufficiently weak for the weak-coupling limit to be valid.[19] We shall take advantage of the equivalence of the macroscopic and microscopic pictures to examine the effects of spin-orbit distortions (not used in the DRC code[7]) by using $L=0$ microscopic form factors in the LOKI coupled-channel code,[20] which does include a spin-orbit optical potential.

Finally, in an attempt to understand the main features of the spin-flip interaction, let us consider the special case of analog transitions for seniority-one states of odd nuclei, where the neutron excess is contained in a single j configuration. Including only the dominant ($L=0$) term, Eq. (2) is reduced to

$$d\sigma/d\Omega = X_0(\theta)\,V_\tau{}^2(N-Z) \times\left[1+\left(\frac{V_{\sigma\tau}}{V_\tau}\right)^2\frac{1}{(N-Z)^2}\begin{cases}(j+1)/j, & j=l+\frac{1}{2}\\ j/(j+1), & j=l-\frac{1}{2}\end{cases}\right] \quad (17)$$

for $j = l\pm\frac{1}{2}$.[21] The first term in Eq. (17) is the single-configuration case of Eq. (13). It can be seen that s states are most strongly affected by spin flip. The coefficients of the spin-flip factor $(j+1)/j$ or $j/(j+1)$

[19] J. J. Wesolowski, E. H. Scharcz, P. G. Roos, and C. A. Ludemann, Phys. Rev. **169**, 878 (1968).

[20] E. H. Scharcz, Phys. Rev. **149**, 752 (1966).

[21] V. A. Madsen and M. J. Stomp (unpublished).

are 3 for $s_{1/2}$, $\frac{5}{3}$ for $p_{3/2}$, $\frac{1}{3}$ for $p_{1/2}$, $\frac{7}{5}$ for $d_{5/2}$, and $\frac{3}{5}$ for $d_{3/2}$. It is clear from these results that the importance of the spin-flip mechanism varies widely from configuration to configuration and, for all cases, is less than the $s_{1/2}$ result.[6] Unless the spin-flip strength is somewhat larger than the spin-independent strength, the spin-flip mechanism will not be very important for ^{13}C and ^{15}N analog transitions. In general, if the neutron excess is large, the spin-flip term will be small.[21] Thus only in the lighter nuclei should one expect to see a significant departure from the $N-Z$ dependence of the Lane model for analog transitions due to spin flip.

Let us next consider the qualitative features of the data. As in previous studies,[3,22] the total cross-section data show strong fluctuations as a function of energy. We believe that these fluctuations are due to doorway-type resonances for which the direct-reaction mechanism does not apply. For this reason we restrict ourselves to the highest energies, where the fluctuations are starting to smooth out.

One of the most striking results is the near equality of the ^{17}O and ^{18}O analog cross sections. The Lane model predicts $\sigma_A(^{18}\mathrm{O})/\sigma_A(^{17}\mathrm{O})\approx 2$, the ratio of the neutron excess. The ^{18}O n_1 group contains, in addition to the analog transition, contributions from several unresolved states. One would therefore expect that, in the absence of the spin-flip mechanism, the ratio of the n_1 group in $^{18}\mathrm{O}(p, n)$ to the $^{17}\mathrm{O}(p, n)$ analog transition would be even greater than the predicted ratio of 2. By comparison with Eq. (17), we see that a spin-flip strength $V_{\sigma\tau}$ comparable to the spin-independent term V_τ is required to give equal ^{17}O and ^{18}O cross sections.

VI. THEORETICAL ANALYSIS

The ^{17}O, ^{18}O, and $^{27}\mathrm{Al}(p, n)$ and other (p, n) angular distributions were calculated using the formalism presented in Sec. IV. The values of the optical parameters used in the calculations are listed in Table I, and the theoretical angular distributions are shown, together with measurements, in Figs. 9–15. The values of V_τ and $V_{\sigma\tau}$ are obtained by normalizing the calculations to the total measured (p, n) cross sections, and are given in Tables II and III. V_τ can be determined independently from the $0^+\rightarrow 0^+$ analog transitions, while $V_{\sigma\tau}$ can be determined from the $0^+\rightarrow 1^+$ transitions as well as from the $\frac{1}{2}^-\rightarrow\frac{3}{2}^-$ $^{15}\mathrm{N}(p, n)$ transition, since the latter is believed to be pure spin flip. These determinations have indicated that $V_{\sigma\tau}$ is slightly weaker than V_τ ($V_{\sigma\tau}\simeq\frac{2}{3}V_\tau$). Analog transitions between states of nonzero spin involve both V_τ and $V_{\sigma\tau}$. For these latter transitions, we have assumed that $V_{\sigma\tau}=\frac{2}{3}V_\tau$. Also included are three pure $\Delta L=2$ transitions which involve both V_τ and $V_{\sigma\tau}$. These are $^{27}\mathrm{Al}(p, n)$ $(\frac{5}{2}^+\rightarrow\frac{1}{2}^+)$, $^{17}\mathrm{O}(p, n)(\frac{5}{2}^+\rightarrow\frac{1}{2}^+)$, and $^{18}\mathrm{O}(p, n)$ $(0^+\rightarrow 2^+)$ (see Fig. 15). In all calculations, the range of the Yukawa two-body force was $\alpha=0.715$ fm^{-1}. This value of range parameter was chosen rather arbitrarily. If $\alpha=1$ has been used, it would affect mainly the relative contributions of $\Delta L=2$ to $\Delta L=0$ transitions, increasing the ratio by a factor of about 1.5. The values of V_τ and $V_{\sigma\tau}$ are mainly sen-

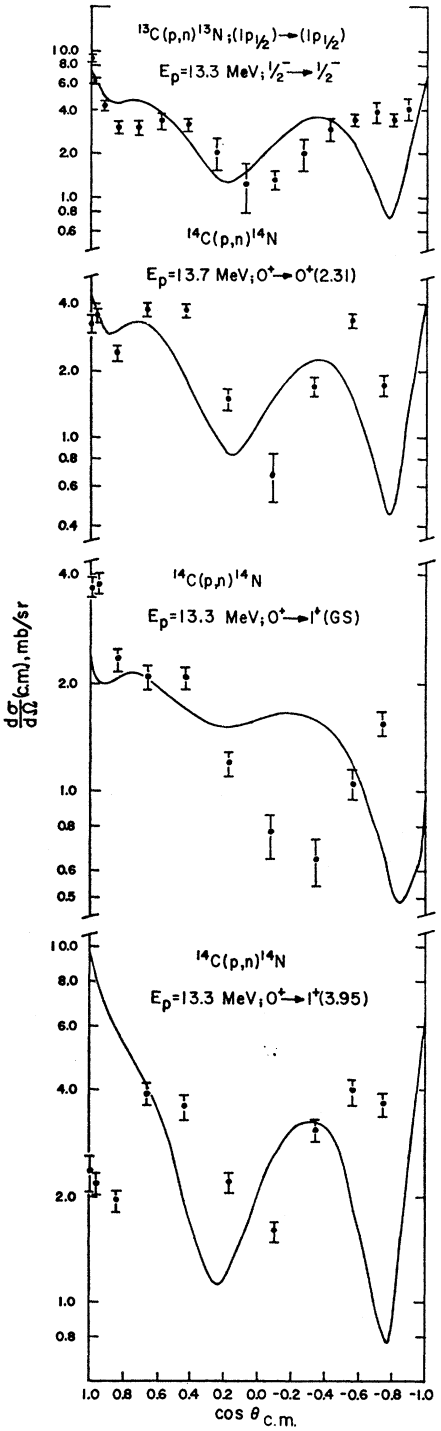

FIG. 9. Theoretical (solid line) and experimental (dots with error bars) angular distributions for $^{13}\mathrm{C}(p, n)^{13}\mathrm{N}$ and $^{14}\mathrm{C}(p, n)^{14}\mathrm{N}$. (Theoretical curves are normalized to experimental total cross sections and are based on the configurations shown, except for ^{14}C, for which Visscher-Ferrell wave functions were used for the theoretical analysis.)

[22] C. Wong, J. D. Anderson, J. W. McClure, and B. Pohl, Phys. Rev. **156**, 1266 (1967).

sitive to the value of the imaginary potential used in the optical model to distort the incoming and outgoing waves. We have made an exhaustive study and believe that the values of the parameters in Table I represent the best estimates based on measurements and/or extrapolations from existing measurements. Under

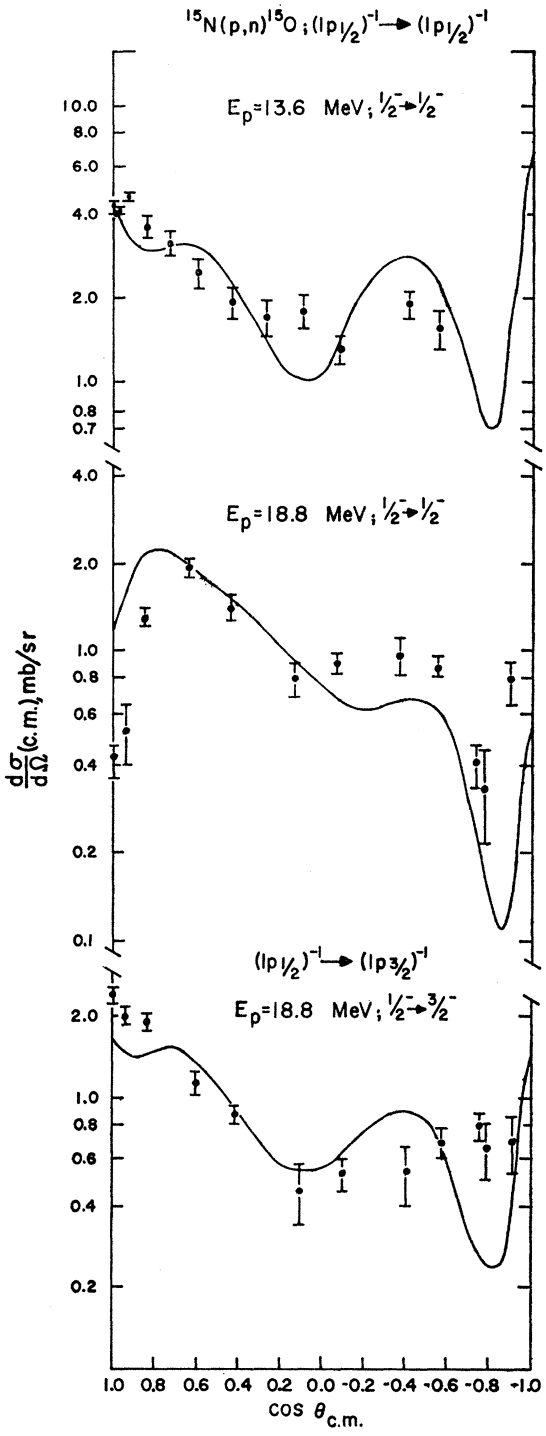

FIG. 10. Theoretical and experimental angular distributions for $^{15}N(p, n)^{15}O$.

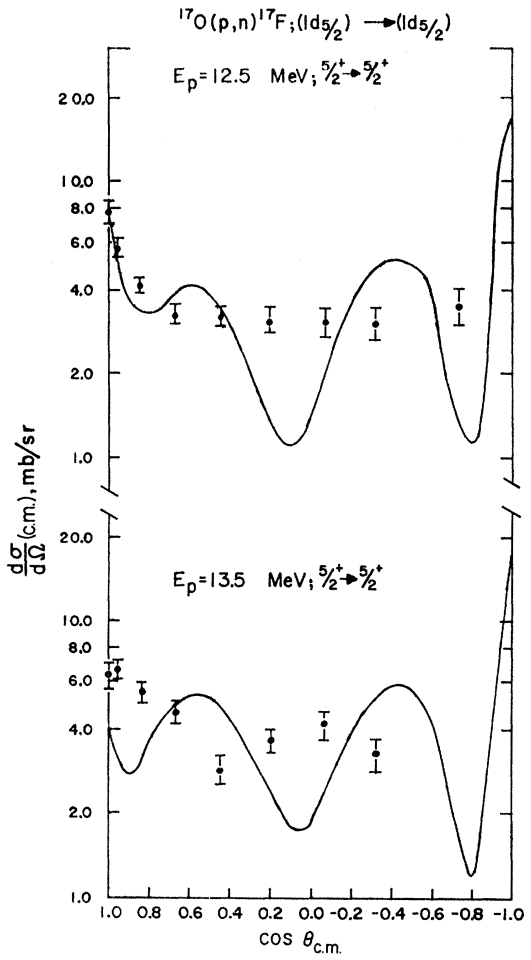

FIG. 11. Theoretical and experimental angular distributions for $^{17}O(p, n)^{17}F$.

"Comments" in Table I we describe briefly how the wave functions and the values of the parameters were determined.[9,23–32] The optical model was assumed to have a Woods-Saxon form for the real potential and a derivative Woods-Saxon for the imaginary potential, i.e.,

$$V_{\text{optical}} = -V(e^x+1)^{-1} - 4iW(d/dx')(e^{x'}+1)^{-1},$$

where

$$x=(r-r_0A^{1/3})/a, \qquad x'=(r-r_0'A^{1/3})/a'.$$

[23] W. M. Visscher and R. A. Ferrell, Phys. Rev. **107**, 781 (1957).
[24] J. Stevens, H. F. Lutz, and S. F. Eccles, Nucl. Phys. **76**, 129 (1966).
[25] R. W. Bauer, J. D. Anderson, H. F. Lutz, C. Wong, J. W. McClure, and B. A. Pohl, Nucl. Phys. **A93**, 673 (1967).
[26] J. D. Anderson, C. Wong, J. W. McClure, and B. D. Walker, Phys. Rev. **136**, B118 (1964).
[27] T. S. Kuo and G. E. Brown, Nucl. Phys. **85**, 40 (1966).
[28] F. G. Perey, Phys. Rev. **131**, 745 (1963).
[29] F. Bjorklund and S. Fernbach, Phys. Rev. **109**, 1295 (1958).
[30] C. D. Goodman, J. D. Anderson, and C. Wong, Phys. Rev. **156**, 1249 (1967).
[31] W. S. Gray, R. A. Kenefick, J. J. Kraushaar, and G. R. Stachler, Phys. Rev. **142**, 735 (1966).
[32] J. D. Anderson and C. Wong (private communication).

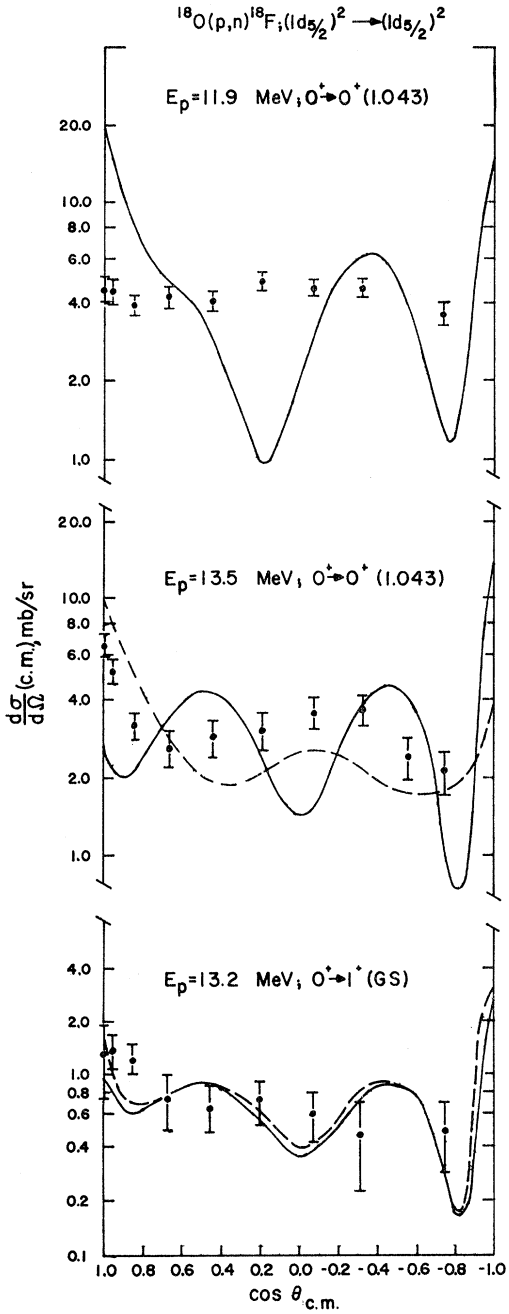

FIG. 12. Theoretical and experimental angular distributions for $^{18}O(p, n)^{18}F$. [The dashed curve for the $0^+ \rightarrow 0^+$ reaction at 13.5 MeV was calculated using the optical code LOKI 2A to illustrate the effect of spin-orbit coupling in reducing the structure in the angular distribution. The dashed curve for the $0^+ \rightarrow 1^+$ (ground-state) reaction was calculated using Kuo-Brown wave functions. It is clear that in changing from the $(1d_{5/2})^2$ configuration (solid curve) to Kuo-Brown wave functions, the effect on the shape of the angular distribution is minimal; however, the value of the total cross section is sensitively affected (see Sec. VIII).]

In Table I the incoming-proton channel parameters are denoted by the subscript p, while the outgoing-neutron channel parameters are denoted by the subscript n. The geometrical parameters, also listed in Table I, vary from nucleus to nucleus and are taken directly from the various references. No attempt has been made to correct the values of V and W to a common set of geometrical parameters. With the exception of the $0^+ \rightarrow 1^+$ transitions in ^{14}C and ^{18}O, the respective initial- and final-state wave functions were assumed to be pure single-particle configurations.

In Sec. V the equivalence of the macroscopic and microscopic descriptions was shown for the weak-coupling limit. We now compare the Lane-model coupled-channel calculations of the differential cross section with those obtained from DWBA. In Fig. 16(a) the radial dependence of g_0^{jj} for ^{18}O is displayed, along with two optical form factors which reasonably approximate the microscopic form factor. The cross sections calculated from DWBA and coupled-channel optical model are shown in Fig. 17(a). From the close agreement, it is clear that we are in the weak-coupling limit, and thus the DWBA is applicable. It also points up the sensitivity of the 0° (p, n) cross section to the

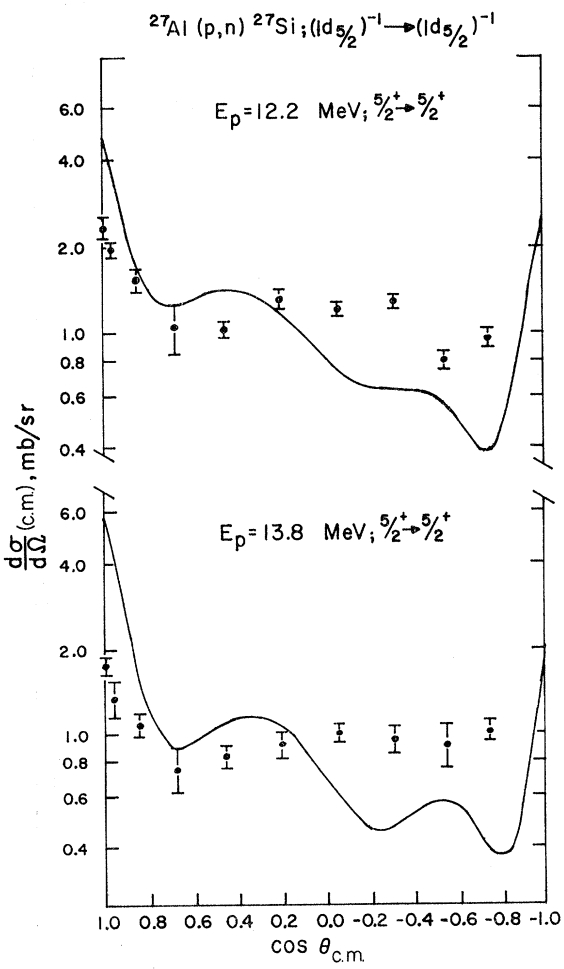

FIG. 13. Theoretical and experimental angular distributions for the $^{27}Al(p, n)^{27}Si$ analog (ground-state) reaction.

TABLE I. Optical parameters.

E_p (MeV)	Target nucleus	Transition	V_p (MeV)	W_p (MeV)	V_n (MeV)	W_n (MeV)	r_{0p} (fm)	a_p (fm)	r_{0p}' (fm)	a_p' (fm)	r_{0n} (fm)	a_n (fm)	r_{0n}' (fm)	a_n' (fm)	Q (MeV)	Comments
13.3	^{13}C	Analog	49.0	6.5	50.0	6.0	1.25	0.65	1.25	0.47	1.25	0.65	1.25	0.47	−3.0	a
13.3	^{14}C	$0^+\rightarrow1^+$ (GS)	46.5	9.0	49.1	5.70	1.25	0.60	1.25	0.47	1.20	0.65	1.20	0.47	−0.6	b
13.7	^{14}C	Analog	46.0	9.0	50.6	6.26	1.25	0.60	1.25	0.47	1.20	0.65	1.20	0.47	−2.93	c
13.3	^{14}C	$0^+\rightarrow1^+$ (3.95 MeV)	46.5	9.0	50.4	4.96	1.25	0.60	1.25	0.47	1.20	0.65	1.20	0.47	−4.55	d
13.6	^{15}N	Analog	52.0	6.2	53.0	6.0	1.25	0.65	1.25	0.47	1.25	0.65	1.25	0.47	−3.5	e
18.8	^{15}N	Analog	46.0	9.1	50.0	7.18	1.25	0.65	1.25	0.47	1.25	0.65	1.25	0.47	−3.5	f
18.8	^{15}N	$\frac{1}{2}^-\rightarrow\frac{3}{2}^-$ (6.15 MeV)	46.0	9.1	53.0	6.0	1.25	0.65	1.25	0.47	1.25	0.65	1.25	0.47	−9.65	g
13.5	^{17}O	Analog	52.0	6.25	50.0	4.16	1.25	0.65	1.25	0.47	1.25	0.65	1.25	0.47	−3.55	h
10.2	^{17}O	$\frac{5}{2}^+\rightarrow\frac{1}{2}^+$ (0.5 MeV)	54.0	5.0	54.0	3.5	1.25	0.65	1.25	0.47	1.25	0.65	1.25	0.47	−4.05	h
12.5	^{17}O	Analog	51.0	5.8	51.0	3.7	1.25	0.65	1.25	0.47	1.25	0.65	1.25	0.47	−3.55	h
10.8	^{17}O	$\frac{5}{2}^+\rightarrow\frac{1}{2}^+$ (0.5 MeV)	52.0	5.5	53.0	4.0	1.25	0.65	1.25	0.47	1.25	0.65	1.25	0.47	−4.05	h
13.2	^{18}O	$0^+\rightarrow1^+$ (GS)	53.0	9.5	50.0	4.2	1.25	0.65	1.25	0.47	1.25	0.65	1.25	0.47	−2.45	i
11.9	^{18}O	Analog	46.3	9.0	50.5	5.0	1.25	0.60	1.25	0.47	1.20	0.65	1.20	0.47	−3.49	j
13.2	^{18}O	$0^+\rightarrow2^+$ (3.06 MeV)	53.0	9.5	50.0	4.5	1.25	0.65	1.25	0.47	1.25	0.65	1.25	0.47	−5.51	j
13.5	^{18}O	Analog	46.3	9.0	50.5	5.0	1.25	0.60	1.25	0.47	1.20	0.65	1.20	0.47	−3.49	j
12.2	^{27}Al	Analog	50.0	8.0	49.0	8.0	1.25	0.65	1.25	0.47	1.25	0.65	1.25	0.47	−5.59	k
10.6	^{27}Al	$\frac{5}{2}^+\rightarrow\frac{1}{2}^+$ (0.78 MeV)	50.0	7.2	53.0	5.0	1.25	0.65	1.25	0.47	1.25	0.65	1.25	0.47	−6.37	k
13.8	^{27}Al	Analog	49.0	8.0	48.0	8.0	1.25	0.65	1.25	0.47	1.25	0.65	1.25	0.47	−5.59	k
15.25	^{48}Ti	Analog	49.4	13.2	45.5	9.5	1.25	0.65	1.25	0.47	1.25	0.65	1.25	0.47	−7.80	l
18.5	^{90}Zr	Analog	52.0	9.25	45.5	9.5	1.20	0.70	1.25	0.65	1.25	0.65	1.25	0.47	−11.8	m

[a] Neutron and proton optical parameters deduced from $^{12}C+p$, $^{12}C+n$, and other light nuclei with appropriate corrections for energy and $\alpha=(N-Z)/A$ dependence. Experimental data from Ref. 3.

[b] Same as c below, except for the use of Visscher-Ferrell wave functions (Ref. 23) for ^{14}C and ^{14}N.

[c] ($^{14}C+p$) parameters taken to be the same as ($^{18}O+p$) (Ref. 24), while ($^{14}N+n$) parameters are taken from Ref. 25. Since $0^+\rightarrow0^+$ transitions are insensitive to configuration mixing, we have assumed the ^{14}C and ^{14}N analog states to be $(p_{1/2})_0^2$. Experimental data from Ref. 9.

[d] Same as c above, except for the use of Visscher-Ferrell wave functions (Ref. 23) for ^{14}C and ^{14}N.

[e] Optical parameters determined as in f below, with experimental data from Ref. 3.

[f] ($^{15}N+p$) parameters deduced from ($^{16}O+p$) and other light nuclei with appropriate corrections for energy and $(N-Z)/A$ dependence. ($^{15}O+n$) parameters deduced from ($^{16}O+n$) and other light nuclei with corrections for energy and $(N-Z)/A$ dependence. Experimental data from Ref. 26.

[g] Optical parameters determined as in f above, while experimental data are unpublished (see Ref. 26).

[h] Optical parameters deduced from ($^{16}O+p$), ($^{16}O+n$), and other light nuclei with appropriate corrections for energy and $(N-Z)/A$ dependence.

[i] Optical parameters determined as in j below. Calculations were made using Kuo-Brown wave functions (Ref. 27) and $(d_{5/2})_{1,0}^2$ single-configuration wave functions.

[j] ($^{18}O+p$) optical parameters taken directly from Ref. 24. ($^{18}F+n$) optical parameters taken to be the same as ($^{14}N+n$) (Ref. 25).

[k] ($^{27}Al+p$) parameters deduced from Perey (Ref. 28). ($^{27}Si+n$) parameters from Bjorklund and Fernbach (Ref. 29).

[l] ($Ti+p$) parameters deduced from Perey (Ref. 28); ($^{48}V+n$) parameters from Bjorklund and Fernbach (Ref. 29). Experimental data from Ref. 30.

[m] ($^{90}Zr+p$) parameters taken from Gray *et al.* (Ref. 31); neutron parameters from Bjorklund and Fernbach (Ref. 29), taking into account the Q of the reaction. Experimental data are unpublished results of Anderson and Wong (Ref. 32).

TABLE II. Analog and pure spin-flip transitions.

E_p (MeV)	Target nucleus	Transition	V_τ	$V_{\sigma\tau}$
13.3	^{13}C	Analog	12.0	8.0
13.7	^{14}C	Analog	9.0	
13.3	^{14}C	$0^+\rightarrow1^+$ (3.95 MeV)		7.3
13.6	^{15}N	Analog	10.3	6.8
18.8	^{15}N	Analog	9.6	6.4
18.8	^{15}N	$\frac{1}{2}^-\rightarrow\frac{3}{2}^-$ (6.15 MeV)	a	6.2
13.5	^{17}O	Analog	11.3	7.5
12.5	^{17}O	Analog	9.1	6.0
13.2	^{18}O	$0^+\rightarrow1^+$ (GS)		4.6[b]
13.2	^{18}O	$0^+\rightarrow1^+$ (GS)		3.6[c]
11.9	^{18}O	Analog	14.2	
13.5	^{18}O	Analog	12.5	
12.2	^{27}Al	Analog	8.9	6.0
13.8	^{27}Al	Analog	8.7	5.8
15.25	^{48}Ti	Analog	9.3	
18.5	^{90}Zr	Analog	8.3	

[a] Insensitive to the value of V_τ, since V_τ contribution requires $\Delta L=2$, which is small compared to $\Delta L=0$ contribution from $V_{\sigma\tau}$.
[b] Pure $(d_{5/2})_{1,0}^2$ wave functions.
[c] Kuo-Brown wave functions.

form factor at large radius. The form factor which falls off faster at large radius gives less scattering at 0°. We now use these results to investigate the importance of the spin-orbit potential which has been neglected in our DWBA calculations (DRC). The results are shown in Fig. 17(b). Although the magnitude of the cross sections is essentially unchanged, the shapes are quite different and in much better agreement with the experimental data [Fig. 12(b)]. Note that these results apply equally well to the ^{17}O calculations, since the form factors are essentially the same, i.e., $d_{5/2}$ single-particle form factors. The results for p-shell nuclei are quite different, in that the inclusion of the spin-orbit term makes much smaller changes in the angular shape. This is gratifying, since the DRC calculations for p-shell nuclei had given a reasonable description of the angular distribution.

It is clear that spin-orbit distortions are important for (p, n) reaction studies, and that their inclusion improves the fit to the data. It is also true that, in calculating effective-interaction constants as in Table I, the inclusion of spin-orbit distortions makes very little difference, since they change the angular distribution without affecting substantially the total cross section. For example, the total cross section in ^{18}O changes by less than 2% when the spin-orbit term is included. Without actually calculating the effects of spin-orbit coupling on the angular distribution, one does not have confidence in the applicability of the reaction model. The fact that the LOKI runs are in reasonable agreement with the experimental data leads us to believe that the direct-reaction model applies and that the effective two-body interaction strengths obtained are meaningful.

In Fig. 16(b) we compare the radial form factor obtained from the microscopic description with the phenomenological form factors usually employed in a macroscopic description. As one might expect, in a light nucleus, where only a single orbit may contribute, the macroscopic description (which implicitly contains an average over many orbits) differs markedly from the microscopic description. It is also gratifying to note that the microscopic calculations, with the inclusion of the spin-orbit distortion, are in better agreement with the experimental data than are the macroscopic calculations [see Fig. 17(c)].

Although the shapes of the angular distributions are somewhat sensitive to optical parameters, the general features are preserved with reasonable variations in the geometrical parameters. If one uses, for example, the parameters of Rosen[33] rather than the parameters pertinent for oxygen, one obtains the results shown

TABLE III. Mainly $\Delta L=2$ transitions.

E_p (MeV)	Target nucleus	Transition	V_τ	$V_{\sigma\tau}$
13.3	^{14}C	$0^+\rightarrow1^+$ (GS)		20.0[a]
10.2	^{17}O	$\frac{5}{2}^+\rightarrow\frac{1}{2}^+$ (0.5 MeV)	19.4	12.9
10.8	^{17}O	$\frac{5}{2}^+\rightarrow\frac{1}{2}^+$ (0.5 MeV)	22.4	15.0
13.2	^{18}O	$0^+\rightarrow2^+$ (3.06 MeV)	27.8	18.5
10.6	^{27}Al	$\frac{5}{2}^+\rightarrow\frac{1}{2}^+$ (0.78 MeV)	13.8	9.2

[a] Visscher-Ferrell wave function.

[33] L. Rosen, J. G. Berry, A. S. Goldhaber, and E. H. Auerbach, Ann. Phys. (N.Y.) **34**, 96 (1965).

in Fig. 17(b). The difference in magnitude of the cross sections is due to the difference in the depth of the imaginary potential. As in all calculations of this type, it should be emphasized again that our estimates of V_τ and $V_{\sigma\tau}$ depend strongly on the imaginary potential assumed for the distorting potential. For our calculations, the relationship is approximated by

$$V_\tau^2 \propto W_n W_p,$$

as was also found by Satchler *et al.*[4]

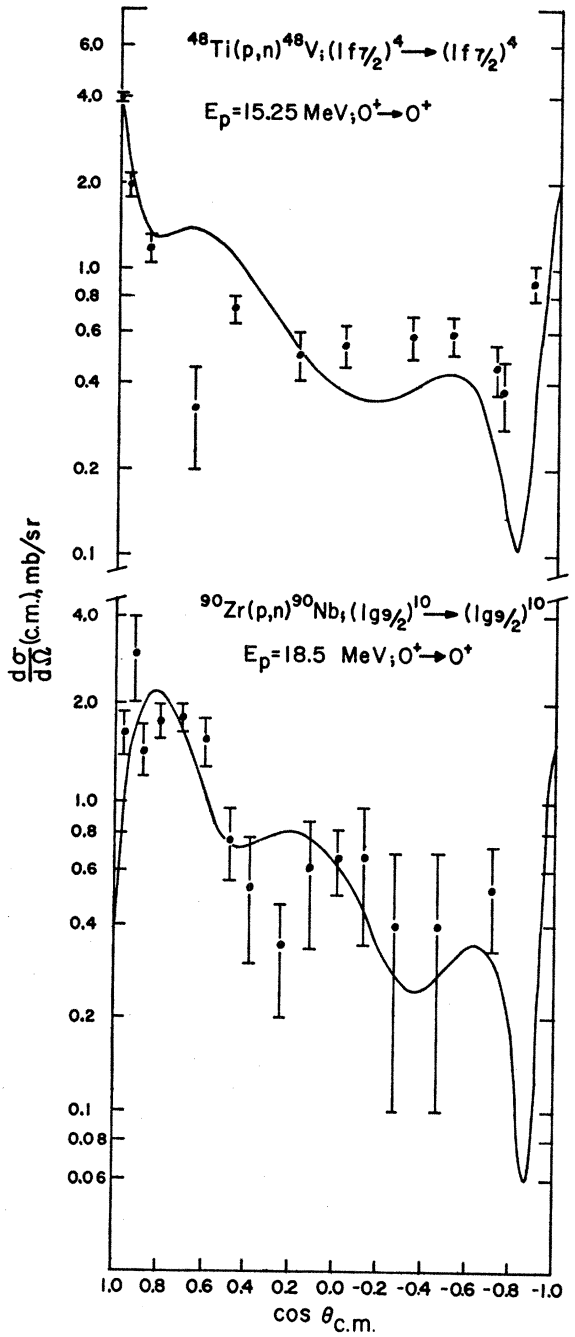

FIG. 14. Theoretical and experimental angular distributions for (p, n) analog reactions ($0^+ \rightarrow 0^+$) in ^{48}Ti and ^{90}Zr.

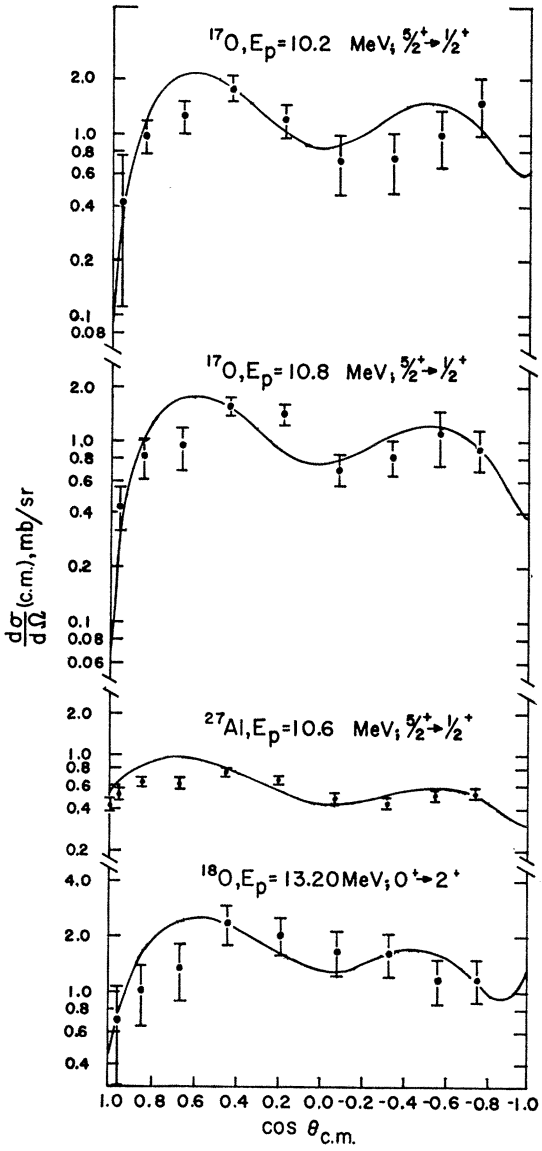

FIG. 15. Theoretical and experimental angular distributions for $L=2$ (p, n) reactions on ^{17}O [$1d_{5/2} \rightarrow 2s_{1/2}$ (0.500 MeV)], ^{27}Al [$1d_{5/2} \rightarrow 2s_{1/2}$ (0.782 MeV)], and ^{18}O [$(1d_{5/2})^2 \rightarrow (1d_{5/2})^2$ (3.058 MeV)].

VII. CONCLUSIONS

All the values of V_τ as deduced from analog transitions for a number of odd and even nuclei, assuming that $V_\tau = \frac{3}{2} V_{\sigma\tau}$, are listed in Table II. Except for ^{18}O, these strengths are reasonably close. Of all cases, the ^{14}C data are the most reliable because the final analog

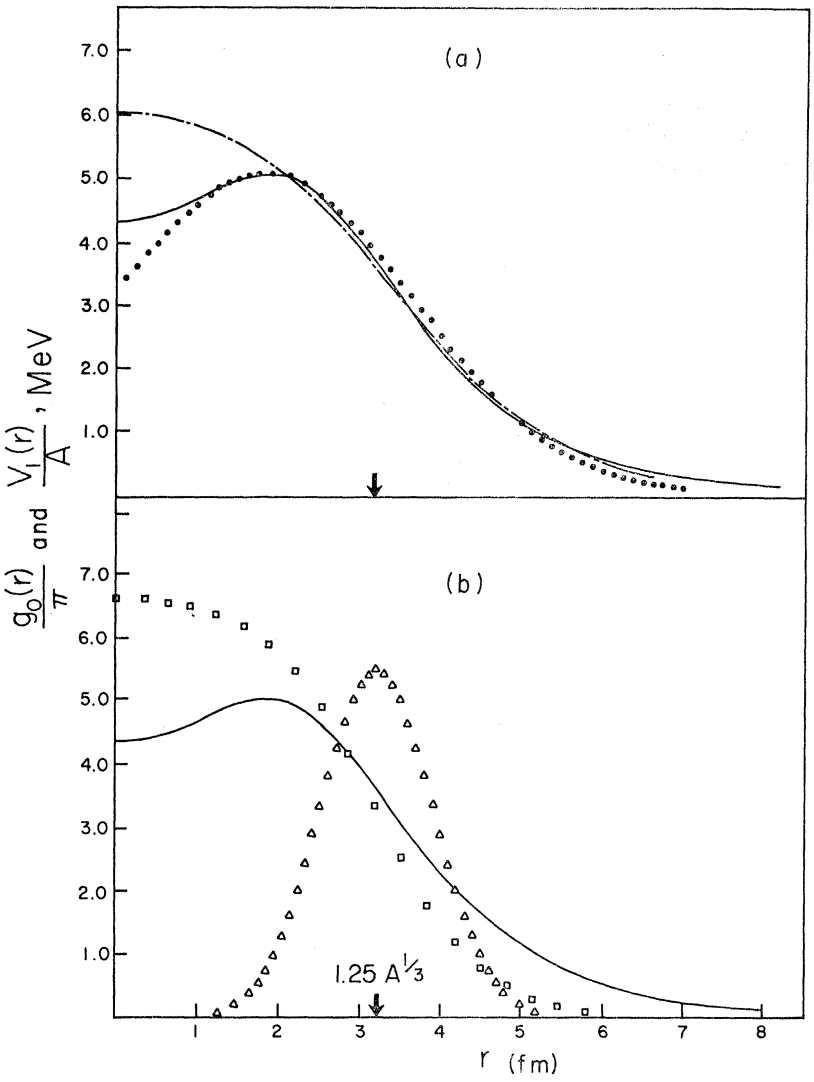

FIG. 16. DRC and LOKI 2A form factors. (a) The solid curve is the DRC form factor $g_0^{5/2,5/2}(r)$ for the $1d_{5/2}$ radial wave function of ^{18}O [see Sec. IV, Eq. (5)]. [The dotted curve is a combined surface and volume isospin potential $V_1(r)$ used in the optical code LOKI 2A, which mocks up the DRC form factor. The dot-dash curve is a pure volume isospin potential, also used in LOKI 2A to mock up the DRC form factor.] (b) The solid curve is the same DRC form factor as in (a). The rectangles (□) are for a "standard" volume isospin potential and the triangles (△) are for a "standard" surface-centered isospin potential, both used in the LOKI 2A optical code.

state is well separated from neighboring states. The case is also a very reliable transition for obtaining V_τ from the standpoint of theory, because, being an $I=0$ transition, it is nearly wave-function-independent. The analog state in the ^{18}O transition cannot be resolved from neighboring states. Contamination from these states is probably responsible for the higher value of V_τ deduced from ^{18}O.

Calculations based on the parameters of Table I should also be capable of explaining other than analog transitions. Tables II and III list the strengths for four pure spin-flip transitions. The ^{14}C$(p, n)^{14}$N ground-state transition would normally be dominated by $L=0$, were it not for the cancellation in matrix elements which makes the β decay rate very nearly zero. The $L=0$ is similarly retarded in the (p, n) reaction.[9] Although the transitions to the 3.95-MeV state of ^{14}N and the 6.18-MeV state of ^{15}O give values for $V_{\sigma\tau}$ in reasonable agreement with those determined from analog transitions, the transitions to the ground states of ^{14}C and ^{18}F are clearly out of line—and in the opposite direction. It is unlikely that inaccuracy in the wave functions is responsible for the difficulty with the ^{14}N ground-state transition, because the Visscher-Ferrell wave functions used in Ref. 9 give a good account of β and electromagnetic transitions. For the transition to the ground state of ^{18}F we have used pure $(1d_{5/2})^2$ wave functions, which are certainly not very accurate. However, the Kuo-Brown configuration-mixed wave functions[27] worsen the agreement by increasing the calculated transition rate to well above the $(1d_{5/2})^2$ result, as they also do for β decay. In fact, the success of the $(1d_{5/2})^2$ configuration in producing approximately the right β decay rate leads us to regard it as more reliable than the wave functions of Ref. 27 for the (p, n) reaction.

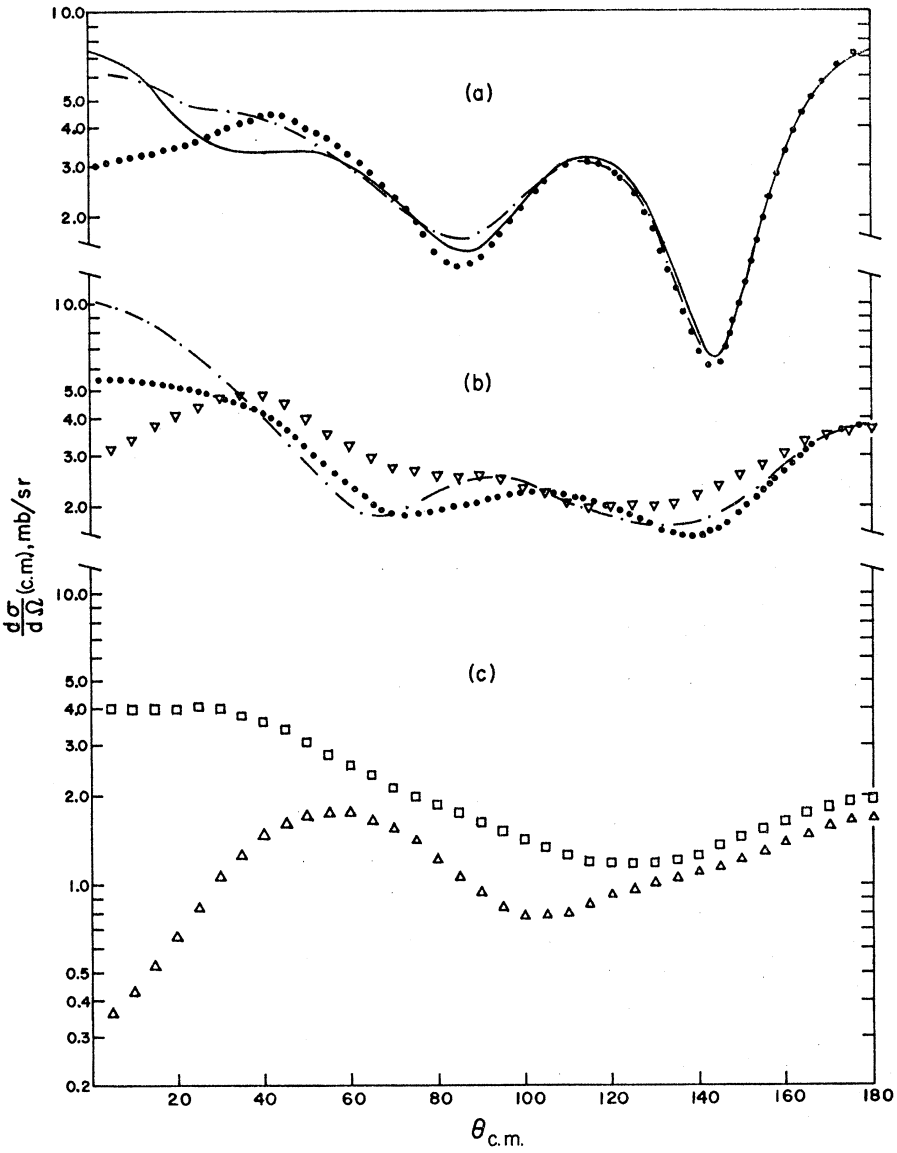

FIG. 17. Theoretical angular distributions corresponding to the form factors used in the DRC microscopic code and the LOKI 2A optical code. (a) The dotted form factors of Fig. 16(a) correspond to the dotted angular distributions of Fig. 17(a), etc. (b) LOKI 2A results for the same parameters as used for the corresponding angular distributions in (a), except for the inclusion of a spin-orbit potential $V_{so}=5.0$ MeV. The additional curve plotted with inverted triangles (∇) was calculated with the Rosen parameters instead of our "standard" parameters (see Sec. VI). The isospin potential $V_1(r)$ was the same as for the dotted curves. (c) LOKI 2A angular distribution corresponding to the isospin form factors of Fig. 16(b).

These arguments lead us to believe that we are seeing a breakdown of the central-interaction no-exchange approximation. Studies of the effects of a possible tensor component to the effective interaction and the effects of particle exchange are underway. One preliminary result of the latter calculations[34] is relevant here—higher L values are enhanced more than lower ones by inclusion of the knockout-exchange amplitudes. This effect would tend to raise the calculated cross section for the ground state of ^{14}N relative to the other transitions. It is unlikely that the exchange will explain entirely the transition to the $^{14}C(p, n)^{14}N$ ground state, however, since knockout exchange does not change qualitatively the angular distributions. The central $L=2$ angular distributions of Ref. 9 failed badly to fit the experiment.

Another interesting pair of nonanalog transitions are the ones to the $\frac{1}{2}^+$ 0.5-MeV state of ^{17}F and the 2^+ 3.06-MeV state of ^{18}F. Both are pure $L=2$ transitions. Calculations based on V_τ of Table II are smaller than the experimental cross section by a factor of 3 for ^{17}F and 5 for ^{18}F. The inclusion of knockout exchange will improve the calculations somewhat, but they will probably still be less than the measured value. This is apparently due to collective enhancement, which, although well established experimentally for transitions in ^{25}Mg, ^{26}Mg, and ^{56}Fe, has not been satisfactorily explained.[22]

[34] A. J. Atkinson and V. A. Madsen, Bull. Am. Phys. Soc. Ser. II, **13**, 630 (1968).

Collective enhancement is well known for inelastic scattering and is understood to be due to core vibration, which interferes constructively with the contribution from extra-core nucleons.[35] The difficulty with this explanation for charge exchange is that the low-lying core-vibrational states, coupled to the extra-core nucleons to form the complete nuclear wave function, are expected to be primarily $T=0$ vibrations. Since the charge exchange must transfer one unit of isospin, it is incapable of exciting such core vibrations. The collective deformed-isospin model used by Satchler[4] essentially treats only these extra-core nucleons (the neutron excess). Two-step processes suggested by Austern and Blair[36] are of the same order as the direct process considered by Satchler[4] and are undoubtedly important. Calculations[37] using the Austern-Blair model[36] have shown enhancements of a factor of 4 due to inclusion of the two-step processes. However, the calculated angular distribution for ^{46}Ti(^{3}He, t) was somewhat poorer than that due to one-step processes alone.[38] Coupled-channel calculations are obviously needed to clarify the role of this mechanism. Another possibility is that there are mixtures of $T=1$ vibrations of the core, brought about by interaction with the extra-core nucleons. These could be excited directly in a one-step process.

The microscopic model of the direct-charge-exchange process is also appropriate for the (^{3}He, t) reaction. The formalism, developed in Ref. 15, has been applied to Ti(^{3}He, t) by Wesolowski *et al.*[19] for 25-MeV ^{3}He particles, to ^{17}O and ^{18}O(^{3}He, t) by Hansen *et al.*[39] at 18 MeV, and to ^{15}N and ^{14}C(^{3}He, t) by Ball and Cerny[40] at 40 MeV. The strengths obtained in the ^{17,18}O experiment are about 20% higher than those we have obtained for $(V_{\sigma\tau}/\alpha^3)$ and about 10% higher for (V_τ/α^3). The Ti(^{3}He, t) reaction yielded a value of V_τ, in good agreement with the ^{17,18}O result. Also, the values obtained from the ^{14}C, ^{15}N experiment are in close agreement with the strengths that we have obtained.

A difficulty in the calculation of the effective-interaction strengths is in our knowledge of optical parameters, particularly the imaginary potential. For each nucleus we have tried to use the best parameters available from optical-model analysis of scattering from the target nucleus or from a neighboring nucleus. However, such scattering data are scarce, and consequently there has been no available systematic study of optical potentials for light nuclei. This is fairly serious for (p, n) reactions, because a symmetry term can result in substantially different neutron and proton potentials. The interaction-strength determinations using DWBA turn out to be fairly sensitive to the imaginary part of the optical potential. Thus a knowledge of the symmetry dependence of the imaginary potential would be of great value in the interpretation of the (p, n) data. The meaningfulness of our results is probably not critically dependent on exchange, since most of our parameters have been obtained for $L=0$ transitions. Preliminary work[41] done at Lawrence Radiation Laboratory, Livermore, Calif., along with the results of Une *et al.*[42] indicate that exchange amplitudes are fairly small for $L=0$ transitions but are by no means negligible.

In spite of these difficulties, the microscopic model with purely central forces is reasonably successful for the analog-state transitions when the spin-flip contribution is included. Comparison of the strengths so obtained with effective interactions obtained in other ways is also of interest. Satchler[1] has calculated the parameter V_τ both by comparing (p, p') with (n, n') data and by fitting Ti, Zr(p, n) data.[1] His analysis yields $V_\tau=$ 20–24 MeV with a Yukawa inverse range parameter $\alpha=1.0$ fm^{-1}. This is equivalent to $V_\tau=7$–8 MeV with our value of $\alpha=0.7$ fm^{-1}. The (p, p') spin-flip transitions are weak, and Satchler was unable to determine values for V_σ and $V_{\sigma\tau}$, but concluded that the over-all spin-flip strength $V_\sigma+V_{\sigma\tau}$ and p,p' was probably somewhat smaller than 10 MeV for $\alpha=1.0$ fm^{-1}. This would correspond to a strength of 3 MeV and is inconsistent with our results, unless V_σ and $V_{\sigma\tau}$ have opposite signs and cancel in the (p,p') reaction.

Also, it is probably worthwhile to compare our parameters with effective forces determined from nuclear-structure calculations using a shell model with purely central interactions. For some time, such a model has had reasonable success in explaining nuclear spectra, and the effective forces arise from the same effects as in the scattering problem. In fact, the success of the shell model for bound states gives us some justification for the use of DWBA with central forces for treating the scattering problem.

In a study of particle-hole states in ^{16}O, Gillet and Vinh Mau[43] have determined an effective strength of $V_\tau=-11.5$ MeV and $V_{\sigma\tau}=-5.5$ MeV for a Gaussian of range $\mu=1.7$ fm. For our Yukawa form with $\alpha=0.7$ fm^{-1} this result is equivalent in volume to $V_\tau=-17.3$ MeV and $V_{\sigma\tau}=-7.4$ MeV. The near-Rosenfeld mixture used by Elliott and Flowers[44] for a study of nuclei of masses 18 and 19 has $V_\tau\approx-4$ MeV and $V_{\sigma\tau}\approx-11$ MeV for an inverse range $\alpha=0.7$ fm^{-1}. These pairs of pa-

[35] W. G. Love and G. R. Satchler, Nucl. Phys. **A101**, 424 (1967).
[36] N. Austern and J. S. Blair, Ann. Phys. (N.Y.) **33**, 15 (1965).
[37] V. A. Madsen, Bull. Am. Phys. Soc. Ser. II, **12**, 907 (1967); W. E. Frahn and G. Weichers, Phys. Letters **26B**, 5 (1967).
[38] V. A. Madsen (private communication).
[39] Luisa F. Hansen, Marion L. Stelts, Jose G. Vidal, J. J. Wesolowski, and V. A. Madsen, Phys. Rev. **174**, 1155 (1968).
[40] G. C. Ball and J. Cerny, Bull. Am. Phys. Soc. Ser. II, **13**, 632 (1968).
[41] A. J. Atkinson and V. A. Madsen, Phys. Rev. Letters **21**, 295 (1968).
[42] T. Une, S. Yamazi, and H. Yoshida, Progr. Theoret. Phys. (Kyoto) **35**, 1010 (1966).
[43] V. Gillet and N. Vinh Mau, Nucl. Phys. **54**, 321 (1964).
[44] J. P. Elliott and B. H. Flowers, Proc. Roy. Soc. (London) **A229**, 536 (1955).

rameters are about the same magnitude as those that we have found, but are not in close agreement, either with our scattering data or with each other.

It is not known whether the comparison between effective nuclear forces from the bound-state problem with those in the scattering problem is really meaningful. Certainly, they arise from similar effects. It is bothersome that the charge-spin-independent term in both the Gillet–Vinh Mau and the Elliott-Flowers interactions is zero or near-zero, since the spin-charge-independent term found by Satchler is much stronger than the charge-exchange force.

We have concentrated on the direct-reaction mechanism as an explanation of the data because it is a reasonably well developed and reliable theory. In doing so, we have not given adequate consideration to the lower-energy data, which show strong fluctuations as a function of energy. Much information about reaction mechanism and nuclear structure is contained in the lower-energy data and could be obtained by analysis with an adequate resonance model. A promising attempt in this direction has been made by Hanna and Nagarajan.[45]

[45] J. S. Hanna and M. A. Nagarajan (unpublished).

PHYSICAL REVIEW VOLUME 177, NUMBER 4 20 JANUARY 1969

Nucleon-Nucleon Scattering from One-Boson-Exchange Potentials. III. S Waves Included*

RONALD BRYAN
Department of Physics, Texas A & M University, College Station, Texas 77843

AND

BRUCE L. SCOTT
Department of Physics-Astronomy, California State College, Long Beach, California 90801

(Received 19 February 1968)

The nucleon-nucleon interaction is described over the laboratory scattering energy range 0–350 MeV by a potential used in conjunction with the Schrödinger equation. In momentum space the potential is a superposition of Born terms obtained from single exchanges of ω, ρ, π, η, σ_0, and σ_1 mesons, where the σ_0 and σ_1 are hypothetical scalar mesons with isotopic spin 0 and 1, respectively. Rather than taking the usual static limit, all terms of order p^2/M^2 are retained. The inclusion of S waves requires the introduction of a cutoff factor. The meson coupling constants, the masses of the σ_0 and σ_1, and a cutoff parameter are adjusted to fit the experimentally determined phase parameters. A comparison with experimental phase-shift analysis shows a good qualitative fit, on the average.

I. INTRODUCTION

THIS is the third in a series of articles[1] whose purpose is to represent the nucleon-nucleon interaction from 0 to 350 MeV in terms of a sum of pole contributions of the ω, ρ, π, η, σ_0, and σ_1 mesons in the cross channel. The requirements of unitarity are satisfied by using the Fourier transform of these pole, or Born, terms as a potential in the nonrelativistic Schrödinger equation. The resulting phase parameters can be compared with experimentally derived phases or used to compute the quantities (cross section, polarization, etc.) which can be directly compared with experiment. The parameters of the theory which are adjusted to fit the data are the coupling constants of all the mesons and the masses of the hypothetical $\sigma_0(T, J^\pi=0, 0^+)$ and the $\sigma_1(1,0^+)$ scalar mesons. We will return to the question of these scalar mesons later in the paper.

In I, a satisfactory fit to the phase parameters was obtained for states with relative orbital angular momenta $l\geq 1$. In that work two important approximations were made. When one transforms the pole terms from momentum to configuration space, the resulting potential is not local (static). An expansion in powers of $\mathbf{p}^2/M^2$, with M the nucleon mass and $\mathbf{p}$ any nucleon momentum, can be made. In I, all terms save one of order $\mathbf{p}^2/M^2$ were kept and the others neglected in order to obtain a local potential. The second important approximation was the introduction of a zero cutoff in configuration space to eliminate the $1/r^3$ divergence in the potential which would have otherwise occurred. The presence of this cutoff restricted the application of the model to P waves and higher.

In II, the aforementioned neglected $\mathbf{p}^2/M^2$ term was now included in the potential, thanks to Green's method[2] for dealing with the resulting $\nabla^2\phi(r)+\phi(r)\nabla^2$ term in configuration space. The inclusion of this $\mathbf{p}^2/M^2$ term

* Much of this work was done at the University of Southern California with the partial support of the U. S. Atomic Energy Commission. This work was also supported in part by the Air Force Office of Scientific Research, Office of Aerospace Research, U. S. Air Force, under Grant No. 918-67.

[1] Ronald A. Bryan and Bruce L. Scott, Phys. Rev. 135, B434 (1964); 164, 1215 (1967), hereafter referred to as I and II, respectively.

[2] A. M. Green, Nucl. Phys. 33, 218 (1962).